

Review of the revised manuscript “Inputs and processes affecting the distribution of particulate Fe in the North Atlantic along the GEOVIDE section” by Gourain, A. and co-authors.

First of all the manuscript has improved massively compared to the last version. The first half of the manuscript is mostly in good shape, but the second part lacks mainly a clear structure of paragraphs which makes it really hard to follow the stream of thoughts. So, especially the conclusion needs to be revisited and strengthened. There is a lot of text, but little information. I am also missing the highlighting of the biogenic fraction, there is hardly anything discussed. However, the data is interpreted and concluded correctly, but changes to the text that need to be done to improve the second part of the paper require between major and intermediate revision. I hope my comments below help to strengthen the text.

With best regards,

Christian Schlosser

Dear Dr Schlosser,

We would like to thank you for your time and effort in this review process.

Concerning the biogenic fraction, it is true that while we are mentioning it in our PMF analysis, we do not discuss it much further, as this is the focus of another paper currently under preparation (distribution between size fractions in the top 200m, completed with chemical leaches analyses). We wrote a specific sentence to mention this lines 358-359.

We reorganized most of the discussion, and simplified some of the wordy sentences.

We truly hope that you will now find this manuscript suitable for publication.

Our detailed answers are below.

Kind regards,

Arthur Gourain, on behalf of all coauthors.

Abstract

Line 35: replace “basins” by “basin” [Done.](#)

Line 36ff: Important sounds strange! I would use “high” instead. Please also include “horizontal”, otherwise advection takes also place vertically. I would also include “advection of PFe containing water masses “ not PFe travels the water mass does this job. [Done.](#)

Line 40ff: This sentence is a bit lost, and out of context. [We removed this sentence.](#)

Method

Line 89: “briefly described in section 2.1” I cannot find a brief description of the complex circulation. [Indeed the circulation is described section 3.1. We changed 2.1 by 3.1 in the text.](#)

Line 102; Remove “and the filters processed...” This is out of context here! [Done.](#)

Line 104: What find of filters you are talking about, these are not filters used for the Swinnex filtration right? [Yes, we are talking about the Swinnex filtration.](#)

Line 133: Replace “filter” by “Filters” Done.

Line 137: You also removed the filter, right? Yes, this is now indicated.

Results

Line 180ff: I have not found any biological settings in this chapter... It is also very long, detailed, and to some extent hard to follow. It would be good to start with a sentence what you are doing and thenm characterize water masses basin after basin separated by different paragraphs. That would make it easier to follow. We removed the biological settings from the title, they were mentioned in the first version of the manuscript and we omit to remove them from the title. We also created more paragraphs to make it easier to follow.

Line 222: This sentence is really hard to understand, please rephrase. Please also shorten the title! We shortened the title as requested to “Open Ocean stations: from the Iberian Abyssal Plain to the Labrador Basin and add an introductory line to precise which stations are concerned by this paragraph. Line 254.

We modified the sentence as follow: “Particulate iron concentration profiles showed identical patterns at all of the open ocean stations encountered along the section.”

Line 229: I have not even watched Figure 3 and sup. Table 1and you introduce Figure 9b and sup. Table 2.
We removed the citation.

Line 253: Include “in THE surface” Done.

Line 281: You refer here to 5 factors, figure 6 represents 4 factors. What is right, I presume the figure?
Indeed 4 factors is the right one.

Line 286: change to “and remineralisation of biogenic material.” Done.

Line 300: Replace “material” by “ fraction”. Done.

Line 312: Replace “with consideration” by “carefully”. Done.

Line 320ff: with %PFe you mean the lithogenic fraction..., be careful and try to apply always the same abbreviation. Indeed there was a typo mistake. It’s been modified to %PFe_{litho}.

Line 320-325: If keeping these sentence, please create a new paragraph. Please also rewrite sentences, they are really hard to understand and follow! Link the %PFe data to Salinity, that at least gives you some certainty that there is a change in water mass. We rewrote this paragraph and included salinity values to demonstrate the presence of the front and thus confirm the link between %PFelitho and salinity value. Lines 344 to 346.

Line 335-340: Please rephrase the sentences, sorry hard to read! Especially the last sentence is formulated very vague! Done

Line 344ff: The following 3 paragraphs should have been included already in section 4.2.You are discussing your results and not discussing them. The structure of the following paragraphs needs to be changed as well, first you come with your hypothesis and then you explain why this is the case. Right now it is all turned around. Why are you coming up with the ratio Mn/Al now. It comes out of the blue. I would introduce this parameter earlier when you come up with %PFe for instance. We are now introducing %PFe litho and %PMn in the methods (section 2.6) as derived parameters. This way, the flow of the discussion is not altered by the explanation of these parameters and flows better. Furthermore, we deleted the subsection title “fingerprinting water masses” and merged the discussion of the water masses exhibiting a specific PFe/PAI with the PMF results and the %PFe litho (lines 380-381;).

Line 379: This paragraph is not explaining the differences of the Fe/Al ratio observed. What is the River doing?

We deleted this paragraph. We were not discussing the PFe/PAI ratio from the water discharge due to the lack of data within the plume and the endmember. The differences of PFe/PAI ratio described line 472 are linked to the margin sediments resuspension.

Line 383: What do you mean with important! We replaced important by high.

Line 396ff: This sentence needs to come first. We reorganized this paragraph.

Line 399ff: Your paragraphs are really long. Anyway, you do not discuss why there are this two maxima. The last sentence “Therefore...” is the most important finding and should come first. And then switching between PFe and PMn, it is hard to follow your stream of thoughts. We reorganized this paragraph.

Line 423ff: What is the message of the paragraph. Buried in the text “Transfer of DFe to PFe. That needs to come in the beginning of the paragraph. We reorganized this paragraph.

Line 479ff: Good this is the most important paragraph, for the first time you put the finding into context and discuss them. It is very hard to go through the last 3 pages without a strong structured line of thoughts!

Thanks, as previously explained, we rewrote the previous paragraph in light of your comments.

Line 494ff: The presented literature data needs to be put in context to your findings towards the end of the following paragraph. We reorganized this paragraph.

Line 526: Include the SEM picture in the sup material. Done.

Line 535ff: First: Barraqueta, Second: What do you mean with the following sentence. It is hard to follow. What has the concentration to do with the composition? We meant that surface waters along the section were not characterised by high concentration of trace metals. We removed to sentence about composition to make the discussion clearer.

Conclusion

This is not a conclusion, it is just a second abstract. We modified the conclusion.

Line 550: Maybe start the Sentence with: The Done.

Line 555: The river is not responsible or the PFe at 2500 m depth. Indeed. We modified the conclusion.

Figure 2 citation: Line 908: Replace “Stations” by “Station” Done.

Figure 3: Please increase the font size of the ODV graphs, it is almost impossible to read the depth and longitude on a print out. Done.

Figure 4 caption: Please include that the PFe scale changes within graphs. Done.

1 **Inputs and processes affecting the distribution of**
2 **particulate iron in the North Atlantic along the GEOVIDE**
3 **(GEOTRACES GA01) section**

4
5
6 Arthur Gourain^{1,2}, Hélène Planquette¹, Marie Cheize^{1,3}, Nolwenn Lemaitre^{1,4}, Jan-Lukas
7 Menzel Barraqueta^{5,6}, Rachel Shelley^{1,76}, Pascale Lherminier⁸⁷ and Géraldine Sarthou¹

8
9 1-UMR 6539/LEMAR/IUEM, [CNRS, UBO, IRD, Ifremer](#), Technopôle Brest Iroise, Place Nicolas Copernic,
10 29280 Plouzané, France

11 2- now at Ocean Sciences Department, School of Environmental Sciences, University of Liverpool, Liverpool,
12 L69 3GP, United Kingdom

13 3- now at Ifremer, Centre de Brest, Géosciences Marines, Laboratoire des Cycles Géochimiques (LCG), 29280
14 Plouzané, France

15 4- now at Department of Earth Sciences, Institute of Geochemistry and Petrology, ETH-Zürich, Zürich,
16 Switzerland

17 5- GEOMAR, Helmholtz Centre for Ocean Research Kiel, Wischhofstraße 1-3, 24148 Kiel, Germany

18 ~~6- now at Department of Earth Sciences, Stellenbosch University, Stellenbosch, 7600, South Africa~~

19 ~~76- now at Earth, Ocean and Atmospheric Science, Florida State University, Tallahassee, Florida, 32310, USA~~

20 ~~87- Ifremer, Univ. Brest, CNRS, IRD, Laboratoire d'Océanographie Physique et Spatiale (LOPS), IUEM, F-~~

21 ~~29280, Plouzané, France; Ifremer, LPO, UMR 6523-CNRS/Ifremer/IRD/UBO, Ifremer Centre de Brest, CS~~

22 ~~40070, Plouzané, France~~

23
24 *Correspondence to: helene.planquette@univ-brest.fr*

25
26 **Abstract**

27 The GEOVIDE cruise (May-June 2014, R/V *Pourquoi Pas?*) aimed to provide a better understanding on trace
28 metal biogeochemical cycles in the North Atlantic. As particles play a key role in the global biogeochemical
29 cycle of trace elements in the ocean, we discuss the distribution of particulate iron (PFe), in light of particulate
30 aluminium (PAI), manganese (PMn) and phosphorus (PP) distributions. Overall, 32 full vertical profiles were
31 collected for trace metal analyses, representing more than 500 samples. This resolution provides a solid basis for
32 assessing concentration distributions, elemental ratios, size-fractionation, or adsorptive scavenging processes in
33 key areas of the thermohaline circulation. Total particulate iron (PFe) concentrations ranged from as low as 9
34 pmol L⁻¹ in surface Labrador Sea waters to 304 nmol L⁻¹ near the Iberian margin, while median PFe
35 concentrations of 1.15 nmol L⁻¹ were measured over the sub-euphotic ocean interior.

36 Within the Iberian Abyssal Plain, ratio of PFe over ~~particulate aluminium~~ (PAI) is identical to the continental
37 crust ratio (0.21), indicating the important influence of crustal particles in the water column. Overall, the

Formatted: Font: Italic

38 lithogenic component explained more than 87% of PFe variance along the section. Within the Irminger and
39 Labrador basins, the formation of biogenic particles led to an increase of the PFe/PAI ratio (up to 0.7 mol mol⁻¹)
40 compared to the continental crust ratio (0.21 mol mol⁻¹). Margins provide ~~important-high~~ quantities of
41 particulate trace elements (up to 10 nmol L⁻¹ of PFe) to the open ocean, and in the case of the Iberian margin,
42 ~~horizontal~~ advection of PFe was visible more than 250km away from the margin. Additionally, several benthic
43 nepheloid layers spreading over 200m above the seafloor were encountered along the transect, especially in the
44 Icelandic, Irminger and Labrador basins, delivering particles with high PFe content, up to 89 nmol L⁻¹ ~~of PFe~~.
45 ~~Finally, remineralisation processes are also discussed, and showed different patterns among basins and~~
46 ~~elements.~~

47 48 1. Introduction

49 Particles play a key role in the ocean where they drive the residence time of most elements (Jeandel ~~and~~
50 ~~Oelkerse~~ et al., 2015), and strongly influence the global biogeochemistry of macro and micro-nutrients including
51 iron (Milne et al., 2017). In the surface ocean, biological activity produces biogenic suspended matter through
52 planktonic organisms, while atmospheric deposition (Baker et al., 2013; Jickells et al., 2005), riverine discharge
53 (Aguilar-Islas et al., 2013; Berger et al., 2008; Ussher et al., 2004) or ice-melting (Hawkings et al., 2014;
54 Lannuzel et al., 2011, 2014) bring mostly lithogenic derived particles to surface waters. These particulate inputs
55 highly vary, both spatially and seasonally, around the world's oceans. At depth, benthic and shelf sediment
56 resuspension (e.g. Aguilar-Islas et al., 2013; Cullen et al., 2009; Elrod et al., 2004; Fitzwater et al., 2000; Hwang
57 et al., 2010; Lam et al., 2015; Lam and Bishop, 2008; McCave and Hall, 2002), and hydrothermal activity
58 (Elderfield and Schultz, 1996; Lam et al., 2012; Tagliabue et al., 2010, 2017; Trefry et al., 1985), provides
59 important amounts of particles to the water column. Moreover, authigenic particles can be produced *in-situ* by
60 aggregation of colloids (Bergquist et al., 2007) or oxidation processes (Bishop and Fleisher, 1987; Collier and
61 Edmond, 1984). Thus, oceanic particles result from a complex combination of these different sources and
62 processes (Lam et al., 2015).

63 Particles represent the main part of the total iron pool in the upper water column (Radic et al., 2011), and
64 strongly interact with the dissolved pool (e.g. Ellwood et al., 2014). Indeed, dissolved iron can be scavenged
65 onto particles (Gerringa et al., 2015; Rijkenberg et al., 2014), incorporated into biogenic particles (Berger et al.,
66 2008) or produced by remineralisation of particles (Dehairs et al., 2008; Sarthou et al., 2008). Interestingly, the
67 concept of "reversible scavenging" (i.e. release at depth of dissolved iron previously scavenged onto particles)
68 has been advocated recently (Dutay et al., 2015; Jeandel and Oelkers, 2015; Labatut et al., 2014), while other
69 studies reveal distinct dissolution processes (e.g. Oelkers et al., 2012; Cheize et al., ~~submitted to Chemical~~
70 ~~Geology~~2018). Slow dissolution of particulate iron at margins has also been evoked as a continuous fertilizer of
71 primary production and should be considered as a source of dissolved iron (e.g. Jeandel et al., 2011; Jeandel
72 and Oelkers, 2015; Lam and Bishop, 2008). Within or below the mixed layer, the rates of regeneration processes can
73 also impact the bioavailable pool of iron, among other trace metals (e.g. Ellwood et al., 2014; Nuester et al.,
74 2014). However, the rates of these processes are not yet fully constrained. The study of particulate iron is thus
75 essential to better constrain ~~the global its marine~~ biogeochemical cycle ~~of iron in the ocean~~. This subject
76 received a growing interest over the last 10 years in particular (e.g. Bishop and Biscaye, 1982; Collier and
77 Edmond, 1984; Frew et al., 2006; Lam et al., 2012; Milne et al., 2017; Planquette et al., 2011, 2013; Sherrell et

78 al., 1998) and, to our knowledge, only two have been performed at an ocean-wide scale and published so far: the
79 GA03 GEOTRACES North Atlantic Zonal Transect (Lam et al., 2015; Ohnemus and Lam, 2015) and the GP16
80 GEOTRACES Pacific Transect (Lam et al., 2017; Lee et al., 2017).

81 In this context, this paper presents the particulate iron distribution in the North Atlantic Ocean, along the
82 GEOTRACES GA01 section (GEOVIDE), and discusses the various sources and processes affecting its
83 distribution, using particulate aluminium, phosphorus or manganese.

84

85 2. Methods

86 2.1. Study area

87 Particulate samples were collected at 32 stations during the GEOVIDE (GEOTRACES GA01 section) cruise
88 between May and June 2014 aboard the R/V *Pourquoi Pas?* in the North Atlantic (Sarthou et al., 2018). The
89 sampling spanned several biogeochemical provinces (Figure 1) that first comprised the Iberian margin (IM,
90 Stations 2, 14 and 14), the Iberian Abyssal Plain (IAP, Stations 11 to 17), the Western European Basin (WEB,
91 Station 19 to Station 29) and the Icelandic Basin (IcB, Stations 32 to 36). Then, samples were collected above
92 the Reykjanes Ridge (RR, Station 38), in the Irminger Basin (IrB, Stations 40 to 60), close to the Greenland
93 shelf (GS, Stations 53, 56 and 61), the Labrador Basin (LB, Stations 63 to 77) and finally close the
94 Newfoundland shelf (NS, Station 78) (Figure 1). The North Atlantic is characterized by a complex circulation
95 (briefly described in section 2.3.1 and in detail by Zunino et al. (2017) and García-Ibáñez et al. (2015) and is one
96 of the most productive regions of the global ocean (Martin et al., 1993; Sanders et al., 2014), with a complex
97 phytoplankton community structure composed of diverse taxa (Tonnard et al., in prep.).

98

99

100

2.2. Sampling

101 Samples were collected using the French GEOTRACES clean rosette, equipped with twenty-two 12L GO-FLO
102 bottles (two bottles were leaking and were never deployed during the cruise). GO-FLO bottles (General
103 Oceanics) were initially cleaned in the home laboratory (LEMAR) following the GEOTRACES procedures
104 (Cutter and Bruland, 2012). The rosette was deployed on a 14mm Kevlar cable with a dedicated, custom-
105 designed clean winch. Immediately after recovery, the GO-FLO bottles were individually covered at each end
106 with plastic bags to minimize contamination. They were then transferred into a clean container (class-100) for
107 sampling and the filters processed under a laminar flow unit. On each cast, nutrient and/or salinity samples were taken to check potential leakage of the GO-FLO
108 bottles.

109 Filters were cleaned following the GEOTRACES protocols (<http://www.geotraces.org/images/Cookbook.pdf>)
110 and kept in acid-cleaned 1 L LDPE bottles (Nalgene) filled with ultrapure water (Milli-Q, resistivity of 18.2 MΩ
111 cm) until use. All filters were 25 mm diameter in order to optimize signal over the filter blank except at the
112 surface depth where 47 mm diameter filters mounted on acid-cleaned polysulfone filter holders (Nalgene™)
113 were used. Prior to filtration, the GO-FLO bottles were shaken three times, as recommended in the
114 GEOTRACES cookbook to avoid settling of particles in the lower part of the bottle. GO-FLO bottles were
115 pressurized to <8 psi with 0.2 μm filtered dinitrogen (N₂, Air Liquide). Seawater was then filtered directly
116 through paired filters (Pall Gelman Supor™ 0.45 μm polyetersulfone, and Millipore mixed ester cellulose MF 5

117 μm) mounted in Swinnex polypropylene filter holders (Millipore), following Planquette and Sherrell (2012)
118 inside the clean container. Filtration was operated until the bottle was empty or until the filter clogged; volume
119 filtered ranged from 2 liters for surface samples to 11L within the water column. After filtration, filter holders
120 were disconnected from the GO-FLO bottles and a gentle vacuum was applied using a syringe in order to
121 remove any residual water under a laminar flow hood. Filters were then removed from the filter holders with
122 plastic tweezers that were rinsed with Milli-Q between samples. Most of the remaining seawater was 'sipped' by
123 capillary action, when placing the non-sampled side of the filter onto a clean 47 mm supor filter. Then, each
124 filter pair was placed in an acid-cleaned polystyrene PetriSlides (Millipore), double bagged, and finally stored at
125 -20°C until analysis at LEMAR. Between casts, filter holders were thoroughly rinsed with Milli-Q, placed in an
126 acid bath (5% Trace metal grade HCl) for 24 hours, then rinsed with Milli-Q.
127 At each station, process blanks were collected as follows: 2L of a deep (1000 m) and a shallow (40 m) seawater
128 samples were first filtered through a 0.2 μm pore size capsule filter (Pall Gelman Acropak 200) mounted on the
129 outlet of the GO-FLO bottle before to pass through the particle sampling filter, which was attached directly to
130 the swinnex filter holder.

131

132

2.3. Analytical methods

133 Back in the home laboratory, sample handling was performed inside a clean room (Class 100). All solutions
134 were prepared using ultrapure water (Milli-Q) and all plasticware had been acid-cleaned before use. Frozen
135 filters, collected within the mixed layer depth or within nepheloid layers, were first cut in half using a ceramic
136 blade: one filter half was dedicated to total digestion (see below), while the other half was archived at -20°C for
137 SEM analyses or acid leaching of "labile" metals (Berger et al., 2008; to be published separately).

138 Filters were digested following the method described in Planquette and Sherrell (2012). Filters were placed on
139 the inner wall of acid-clean 15mL PFA vials (Savillex™), and 2 mL of a solution containing 2.9 mol L⁻¹
140 hydrofluoric acid (HF, suprapur grade, Merck) and 8 mol L⁻¹ nitric acid (HNO₃, Ultrapur grade, Merck) was
141 added to each vial. Vials were then closed and refluxed at 130°C on a hot plate for 4 hours and filters removed.
142 After cooling, the digest solution was evaporated at 110°C until near dryness. Then, 400 μL of concentrated
143 HNO₃ (Ultrapur grade, Merck) was added, and the solution was re-evaporated at 110°C. Finally, the obtained
144 residue was dissolved with 3mL of a 0.8 mol L⁻¹ HNO₃ (Ultrapure grade, Merck). This archive solution was
145 transferred to an acid cleaned 15 mL polypropylene centrifuge tube (Corning®) and stored at 4°C until analyses.
146 All analyses were performed on a sector field inductively coupled plasma mass spectrometer (SF-ICP-MS
147 Element2, Thermo-Fisher Scientific). Samples were diluted by a factor of 7 on the day of analysis in acid-
148 washed 13 mm (outer diameter) rounded bottom, polypropylene centrifuge tubes (VWR) with 0.8 mol L⁻¹ HNO₃
149 (Ultrapur grade, Merck) spiked with 1 μg L⁻¹ of Indium (¹¹⁵In) solution in order to monitor the instrument drift.
150 Samples were introduced with a PFA-ST nebulizer connected to a quartz cyclonic spray chamber (Elemental
151 Scientific Incorporated, Omaha, NE) via a modified SC-Fast introduction system consisting of an SC-2
152 autosampler, a six-port valve and a vacuum-rinsing pump. The autosampler was contained under a HEPA
153 filtered unit (Elemental Scientific). Two 6-points, matrix-matched multi-element standard curves with
154 concentrations bracketing the range of the samples were run at the beginning, the middle and the end of each
155 analytical run. Analytical replicates were made every 10 samples, while accuracy was determined by performing
156 digestions of the certified reference material BCR-414 (plankton, Community Bureau of Reference,

Field Code Changed

157 Commission of the European Communities), PACS-3 and MESS-4 (marine sediments, National Research
158 Council Canada), following the same protocol as for samples. Recoveries were typically within 10% of the
159 certified values (and within the error of the data, taken from replicate measurements, Table 1). Once all data
160 were normalized to an ¹¹⁵In internal standard and quantified using an external standard curve, the dilution factor
161 of the total digestion was accounted for. Obtained element concentrations per filter (pmol/filter) were then
162 corrected by the process blanks described above. Finally, pmol/filter values were divided by the volume of
163 water filtered through stacked filters.

164 Total concentrations (sum of small size fraction (0.45-5 µm) and large (>5 µm) size fraction) of particulate trace
165 elements are reported in Table S1 (~~supplementary data~~).

166

167

2.4. Ancillary data:

168 ~~Potential temperature (θ), salinity (S), and transmissometry data were retrieved from the CTD sensors (CTD~~
169 ~~SBE911 equipped with a SBE43).~~

170

171

2.5.4. Positive matrix factorisation

172 Positive Matrix Factorisation (PMF) was run to characterise the main factors influencing the particulate trace
173 elements variances along the GEOVIDE section. In addition to PFe, PAI, PMn, and PP, nine additional
174 elements were included in the PMF: Y, Ba, Pb, Th, Ti, V, Co, Cu and Zn. The analysis has been conducted on
175 samples where all the 13 elements previously cited were above the detection limits; after selection, 445 of the
176 549 existing data points were used. Analyses were performed using the PMF software, EPA PMF 5.0,
177 developed by the USA Environmental Protection Agency (EPA). Models have been tested with several factors
178 number (from 3 to 6), after full error estimation of each model, we decide to use the configuration providing the
179 lowest errors estimations and in consequence the most reliable.

180 In consequence, models were set up with four factors and were run 100 times to observe the stability of the
181 obtained results. After displacement, error estimations and bootstraps error estimations, the model was
182 recognised as stable.

183

184

2.6.5. Derived and ancillary parameters

185 ~~To investigate The PFe/PAI ratio can be used to estimate the proportion of lithogenic particles iron within the~~
186 ~~bulk particulate fraction, we use. A comparison with the Upper Continental Crust (UCC) Fe/Al molar ratio of~~
187 ~~Taylor and McLennan (1995), 0.21, was used to calculate the lithogenic components of particles (%PFe_{litho})~~
188 ~~following Eq. (1):~~

189

190

$$\%PFe_{litho} = 100 * \left(\frac{PAI}{PFe}\right)_{sample} * \left(\frac{PFe}{PAI}\right)_{UCC \text{ ratio}} \quad (1)$$

191

192 ~~Then the non-lithogenic PFe is simply obtained using Eq. (2):~~

193

194

$$\%PFe_{non_litho} = 100 - \%PFe_{litho} \quad (2)$$

195
196 ~~Note that while (Both the lithogenic and non-lithogenic fraction of PFe are estimated using the UCC ratio. Spatial and temporal variation of the lithogenic components ratio may falsely influence the estimated fraction value. The %PFe_{litho} and %PFe_{non-litho} proxies are interesting tools to evaluate the importance of lithogenic and non-lithogenic (either biogenic or authigenic), but they have to be used carefully, as spatial and temporal variation of the lithogenic component ratios may falsely influence the estimated fraction value.~~

201
202 In addition to PAI, PMn can be used as a tracer of inputs from shelf resuspension (Lam and Bishop, 2008).
203 Indeed, Mn is really sensitive to oxidation mediated by bacteria (Tebo et al., 1984; Tebo and Emerson, 1985)
204 and forms manganese oxides (MnO₂). These authigenic particles lead to an enrichment of Mn in particle
205 compositions. In order to track the influence of shelf resuspension, a percentage of sedimentary inputs “%bulk
206 sediment inputs” can be estimated using PMn/PAI ratio from GEOVIDE samples and the PMn/PAI UCC value
207 (0.0034; Taylor and McLennan, 1995) according to the following equation:

$$\% \text{bulk sediment PMn} = 100 * \left(\frac{\text{PAI}}{\text{PMn}} \right)_{\text{sample}} * \left(\frac{\text{PMn}}{\text{PAI}} \right)_{\text{UCC ratio}} \quad (3)$$

209 This proxy ~~is~~ can be a good indicator of direct and recent sediment resuspension. We assume that particles
210 newly resuspended in water column will have the same PMn/PAI ratio than the UCC ratio leading to a “%bulk
211 sediment Mn” of 100%. This value will decrease by authigenic formation of Mn oxides. This proxy assumes
212 homogeneity of the sediment PMn/PAI ratio through the section which ~~is~~ maybe not be completely the case at
213 every station. In consequence, this proxy is only a tool to identify new benthic resuspension at specific location
214 and inter-comparison between several locations is not possible. When a sample presents a “%bulk sediment
215 Mn” greater than 100%, we assign a value of 100% to simplify the following discussion. As the Mn cycle can
216 also be affected by biologic uptake (e.g. Peers and Price, 2004; Sunda and Huntsman, 1983), this proxy is only
217 used at depths where biologic activity is negligible (i.e. below 150m depth).

218 Potential temperature ($\theta^{\circ}\theta$), salinity (S), and transmissometry data were retrieved from the CTD sensors (CTD
219 SBE911 equipped with a SBE43).

Formatted: Font: Italic

222 3. Results

223 3.1. Hydrography and biological setting

224 Here, we briefly describe the hydrography encountered during the GEOVIDE section (Figure 2), as a thorough
225 description is available in García-Ibáñez et al. (2015). In the beginning of the section-, The warm and salty
226 Mediterranean Water (MW, S=36.50, θ° =11.7°C) was sampled between 600 and 1700 m in the Iberian Abyssal
227 Plain (IAP). MW resulted from the mixing between the Mediterranean Overflow Water plume coming from the
228 Mediterranean Sea and local waters. Surface water above the Iberian Shelf was characterised by low salinity
229 (S=34.95) at station 2 and 4 compared to surrounding water masses. Close to the floor of the Iberian Abyssal
230 Basin, the North East Atlantic Deep Water (NEADW, S=34.89, θ° =2.0°C) spread southnorthward. The North
231 Atlantic Central Water (NACW, S>35.60, θ° >12.3°C) was the warmest water mass of the transect and was

232 observed in the subsurface layer of the Western European Basin and Iberian Abyssal Plain. An old Labrador Sea
233 Water (LSW, $S=34.87$, $\theta=3.0^{\circ}\text{C}$) flowed inside the Western European and Icelandic Basins, between 1000 and
234 2500m depth.

235 -In the Icelandic Basin, below the old LSW, the Iceland-Scotland Overflow Water (ISOW, $S=34.98$, $\theta=2.6^{\circ}\text{C}$)
236 spread along the Reykjanes Ridge slope. This cold water, originating from the Arctic, led to the formation of
237 NEADW after mixing with surrounding waters. North Atlantic hydrography was impacted by the northward
238 flowing of the North Atlantic Current (NAC), which carried up warm and salty waters from the subtropical area.
239 By air-sea interactions and mixing with surrounding water, the NACW is cooled down and freshened in the
240 subpolar gyre and is transformed in Subpolar Mode Water (SPMW).When NAC crossed the Mid-Atlantic ridge
241 through the Charlie-Gibbs Fracture Zone (CGFZ), it created the Subpolar Mode Water (SPMW). The
242 recirculation-formation of SPMW inside the Icelandic and Irminger Basins led to the formation of regional
243 modal waters: the Iceland Subpolar Mode Water (IcSPMW, $S=35.2$, $\theta=8.0^{\circ}\text{C}$) and the Irminger Subpolar Mode
244 Water (IrSPMW, $S=35.01$, $\theta=5.0^{\circ}\text{C}$) respectively. IcSPMW was a relatively warm water mass with potential
245 temperature up to 7°C (García-Ibáñez et al., 2015). Another branch of the NAC mixed with Labrador Current
246 waters to form the relatively fresh SubArctic Intermediate Water (SAIW, $S<34.8$, $4.5^{\circ}\text{C}<\theta<6^{\circ}\text{C}$).

247 The Irminger Basin is a complex area with a multitude of water masses. In the middle of the basin, an old LSW,
248 formed one year before (Straneo et al., 2003), spread between 500 and 1200 m depth. Close to the bottom, the
249 Denmark Strait Overflow Water (DSOW, $S=34.91$) flowed across the basin. Greenland coastal waters were
250 characterised by low salinity values, down to $S=33$. The strong East Greenland Current (EGC) flowed
251 southward along the Greenland shelf in the Irminger Basin. When reaching the southern tip of Greenland, this
252 current entered the Labrador Basin along the west coast of Greenland and followed the outskirts of the basin
253 until the Newfoundland shelf. In the Labrador Basin, the deep convection of SPMW at 2000 m was involved in
254 the formation of the LSW ($S=34.9$, $\theta=3.0^{\circ}\text{C}$) (García-Ibáñez et al., 2015; Yashayaev and Loder, 2009).
255 Above the Newfoundland Shelf, surface waters were affected by discharge from rivers and ice-melting and
256 characterised by extreme low salinity for open ocean waters, below 32 in the first 15 meters.

257 3.2. Section overview

258 Total particulate iron-(PFe), aluminium-(PAI), manganese-(PMn) and phosphorus-(PP) concentrations spanned a
259 large range of concentrations from below detection to 304, 1544, -3.5 and 402 nmol L⁻¹ respectively. The ranges
260 of concentrations are comparable to other studies recently published (Table 2).

261 PFe, PAI, and PMn were predominantly found (>90%) in particles larger than 5 μm , except in surface waters,
262 where $9 \pm 8.6\%$ of PFe, ~~$38.8 \pm 8.6\%$ of PP~~, $10.9 \pm 15.4\%$ of PAI and $32.8 \pm 16.6\%$ of PMn, ~~$38.8 \pm 8.6\%$ of~~
263 ~~PP~~ were hosted by smaller particles (0.45-5 μm). ~~The ranges of concentrations are comparable to other studies~~
264 ~~recently published (Table 2).~~ Data are shown in Figure 3.

265

266 3.3. Open Ocean stations -stations: from the Iberian Abyssal Plain (stations 11 to 17);
267 Western European Basin (stations 19 to 29); Icelandic Basin (stations 32 to 36); Reykjanes Ridge
268 (station 38); Irminger Basin (stations 40 to 60); except Stations 53 and 56) and to the Labrador Basin
269 (stations 63 11 to 77, except stations 53, 56 and 61)

270 This concerns all stations ~~between~~from station 11 to 77, with the exception of stations 53, 56 and 61 that were
271 ~~sampled close to the Greenland and Newfoundland coast (Figure 1)s, respectively.~~
272 Particulate iron concentration ~~vertical~~ profiles ~~presented~~ ~~showed~~ identical patterns at ~~all of the~~ open ocean
273 stations ~~sampled in each oceanic basin~~ encountered along the section. Median PFe were low at 0.25 nmol L⁻¹
274 within the first 100 m and steadily increased with depth. However, at two stations, elevated concentrations were
275 determined in the upper 100m, up to 4.4 nmol L⁻¹ at station 77 at 40 m and 7 nmol L⁻¹ at station 63 between 70
276 and 100 m depth. PFe concentrations gradually increased with depth, with a median PFe of 1.74 nmol L⁻¹ below
277 1000m. Close to the seafloor of some stations (26, 29, 32, 34, 49, 60, and 71), high concentrations of PFe were
278 observed, up to 88 nmol L⁻¹ (station 71 at 3736 m). These high PFe values were associated with low beam
279 transmissometry value inferior or equal to 97.7%. ~~(Figure 9b and supplementary table S2).~~
280 Particulate aluminium (PAI) and manganese (PMn) profiles were similar to PFe profiles, with low
281 concentrations measured in the first 100 m (1.88 nmol L⁻¹ and 55 pmol L⁻¹, respectively) and increased towards
282 the seafloor. Close to the seafloor, high concentrations were determined at the same stations cited above for PFe,
283 with a maximum of 264 nmol L⁻¹ and 3.5 nmol L⁻¹ for PAI and PMn respectively at station 71 (supplementary
284 Table S1). Highest particulate phosphorus (PP) concentrations were in the first 50m, with a median value of 66
285 nmol L⁻¹. Deeper in the water column, below 200m, PP concentrations decreased to values below 10 nmol L⁻¹.
286 Inter-basins differences were observed within the surface samples, with median PP concentration being higher
287 in the Irminger Basin (127 nmol L⁻¹) than in the Iberian Abyssal Plain (28 nmol L⁻¹) ~~(Figure 3).~~
288 Finally, above the Reykjanes Ridge, PP, PMn, PAI and PFe concentrations were in the same range than the
289 surrounding open ocean stations. However, close to the seafloor, high concentrations were measured, with PFe,
290 PAI, and PMn reaching 16.2 nmol L⁻¹, 28.8 nmol L⁻¹, and 0.51 nmol L⁻¹ at 1354 m, respectively (Figure 3 and
291 ~~supplementary material~~ Table S1).

292

293 *3.4. Margins and Shelves: Iberian Margin (stations 1 to 4), Greenland coast (stations 53, 56*
294 *and 61) and Newfoundland Shelf (station 78)*

295

296 The Iberian margin was characterised by low beam transmissometry values at station 2 (88% at 140 m, Figure
297 49b) suggesting significant particle concentrations. Particulate iron concentrations varied between 0.02 nmol L⁻¹
298 to 304 nmol L⁻¹. Within the first 50m, PFe concentrations decreased towards the shelf break where PFe dropped
299 down from 2.53 nmol L⁻¹ (station 2) to 0.8 nmol L⁻¹ (Station 1). ~~At tall three stations,~~ PFe concentrations
300 increased with depth ~~at all three stations~~ and reached a maximum ~~at the be~~close to the seafloor. ~~As an exemple,~~
301 ~~300 nmol L⁻¹ of PFe was measured at 138.5m at ttom of station 2 (138.5 m) with more than 300 nmol L⁻¹ of~~
302 ~~PFe.~~ Lithogenic tracers, such as PAI or PMn, presented similar profiles to PFe with concentrations ranging
303 between 0.11 and 1544 nmol L⁻¹, and from below detection limit to 2.51 nmol L⁻¹ respectively (Figure 3,
304 ~~supplementary material~~ Table S1). Total particulate phosphorus (PP) concentrations were relatively low in ~~the~~
305 surface ranging from undetectable values to 38 nmol L⁻¹; concentrations decreased with depth and were less
306 than 0.7 nmol L⁻¹ below 1000 m depth.

307 In the vicinity of the Greenland shelf, PFe concentrations had a high median value of 10.8 nmol L⁻¹ and were
308 associated with high median PAI and PMn concentrations of 32.3 nmol L⁻¹ and 0.44 nmol L⁻¹, respectively.
309 Concentrations of PP were high at the surface with a value of 197 nmol L⁻¹ at 25 m of station 61. Then, PP

Formatted: Superscript

310 concentrations decreased strongly, less than 30 nmol L⁻¹, below 100 meters depth. Furthermore, beam
311 transmissometry values in surface waters at these three stations, were the lowest of the entire section, with
312 values below 85%.

313 Close to the Newfoundland margin, surface waters displayed a small load of particulate trace metals as PFe,
314 PAI, and PMn were below 0.8 nmol L⁻¹, 2 nmol L⁻¹, and 0.15 nmol L⁻¹ respectively. Then close to the bottom of
315 station 78, at 371 m, beam transmissometry values dropped to 94% and were associated with extremely high
316 concentrations of PFe=168 nmol L⁻¹, PAI=559 nmol L⁻¹, and PMn=2 nmol L⁻¹. Total PP concentrations in the
317 first 50 m ranged from 35 to 97 nmol L⁻¹. Below ~~the surface~~, PP remained relatively high with values up to 16
318 nmol L⁻¹ throughout the water column. (Figure 3 and ~~supplementary material~~-Table S1).

319

320 4. Discussion

321 Our goal in this work was to investigate mechanisms that drive the distribution of PFe in the North Atlantic, in
322 particular the different routes of supply and removal. Possible candidate sources of PFe include lateral advection
323 offshore from margins, atmospheric inputs, continental run-off, melting ice shelves and icebergs, resuspended
324 sediments, hydrothermal inputs and biological uptake. Removal processes include remineralization, ~~and~~
325 dissolution processes ~~and sediment burial~~.

326 In the following sections, we examine each of these sources and processes, explore the evidence for their
327 relative importance, and use compositional data to estimate the particle types and host phases for iron and
328 associated elements.

329 *4.1. Analysis of the principal factors controlling variance: near-ubiquitous influence of* 330 *crustal particles in the water column*

331 ~~The positive matrix factorisation analysis (Figure 5) has been realised on the entire dataset, in consequence, the~~
332 ~~factors described below are highly influenced by the major variations of particulate element concentrations~~
333 ~~(usually at the interface, i.e. margin, seafloor, surface layer). The positive matrix factorisation, shown in Figure~~
334 ~~5, indicate factorisation, shown in Figure 5, indicates the overall variances explained by each of the 45 factors.~~

335 The first factor is characterised by lithogenic elements, representing 86.8% of the variance of PFe, 75.8% of PAI
336 and 90.5% of PTi. The second factor is correlated with both Mn and Pb and explains no less than 76.5% and
337 77.0% of their respective variances. Ohnemus and Lam (2015) observed this co-relation between manganese
338 and lead particles and explained it by the co-transport on Mn-oxides (Boyle et al., 2005). The formation of barite
339 is causing the third factor constraining 87.7% of the Ba variance in the studied regions. Biogenic barite
340 accumulation within the mesopelagic layer is related to bacterial activity and ~~organic~~-remineralisation of
341 ~~biogenic material~~ (Lemaitre et al., 2018a). A biogenic component is the fourth factor and explained most of
342 particulate phosphorus variance, 83.7%. The micronutrient trace metals, copper, cobalt and zinc, had more than
343 a quarter of their variances influenced by this factor. ~~Note that t~~The biogenic contribution to particulate iron and
344 ~~other particulate-trace elements will be discussed in another paper (Planquette et al., in prep).~~

345 These results indicate that along the GA01 section, PFe distributions were predominantly controlled by
346 lithogenic material and to a smaller extent by remineralisation processes (as seen by a Factor 3 contribution of
347 4.1%). This does not rule out some biogenic influence on PFe distribution, especially in surface, but this
348 contribution is veiled by the high lithogenic contribution. ~~The PMF analysis has been realised on the entire~~

349 dataset, in consequence, the factors described are highly influenced by the major variations of particulate
350 element concentrations (usually at the interface, i.e. margin, seafloor, surface layer,...).

351 To further investigate the influence of crustal material on the distribution of PFe, it is instructive to examine the
352 distribution of the molar ratio of PFe/PAI, and the resulting %PFe_{litho} (see section 2.6 for definition of this
353 parameter) along the section as a way to assess the lithogenic inputs (Lannuzel et al., 2014; Ohnemus and Lam,
354 2015; Planquette et al., 2009) (Figure 6) along the section.

355 The PFe/PAI ratio can be used to estimate the proportion of lithogenic particles within the bulk particulate
356 material. A comparison with the Upper Continental Crust (UCC) ratio of Taylor and McLennan (1995), 0.21,
357 was used to calculate the lithogenic components of particles (PFe_{litho}) following Eq. (1):

$$358 \quad \%PFe_{litho} = 100 * \left(\frac{PAI}{PFe}\right)_{sample} * \left(\frac{PFe}{PAI}\right)_{UCC \text{ ratio}} \quad (1)$$

361 Then the non-lithogenic PFe is simply obtained using Eq. (2):

$$362 \quad \%PFe_{non_litho} = 100 - \%PFe_{litho} \quad (2)$$

365 Both the lithogenic and non-lithogenic fraction of PFe are estimated using the UCC ratio. Spatial and temporal
366 variation of the lithogenic components ratio may falsely influence the estimated fraction value. The PFe_{litho} and
367 PFe_{non-litho} proxies are interesting tools to evaluate the importance of lithogenic and non-lithogenic (either
368 biogenic or authigenic), but have to be used with consideration.

369 Overall, the estimated lithogenic contribution to PFe varies from 25% (station 60, 950 m) to 100% at stations
370 located within the Western European Basin. Note that 100% of estimated lithogenic PFe does not necessary
371 mean that biogenic particles are absent; they may just be masked by the important load of lithogenic particles.
372 Important inter-basins variations are observed along the section (Figure 6). The IAP and WEB basins are linked
373 with high median value of the proxy %PFe_{litho}, 90%, which is also reflected in the MW and NEADW PFe/PAI
374 ratio, that displays a value PFe/PAI close to the crustal one (Figure 7). This
375 could be linked to a lateral advection of iron rich lithogenic particles sourced from the Iberian margin and to
376 atmospheric particles (Shelley et al., 2017). This point is discussed with more detail in section 4.3.4. Then,
377 between the stations 26 and 29, the %PFe_{litho} proxy values dramatically decreased, and reached values under
378 55%; between the stations 26 and 29, to reach median %PFe_{litho} value under 55% in the Iceland, Irminger and
379 the Labrador basins. This feature is likely be associated to the presence of the Sub-Arctic Front, located between
380 49.5 and 51°N latitude and 23.5 and 22°W longitude (Zunino et al., 2017). Indeed, this front which separates
381 cold and fresh water of subpolar origin from warm and salty water of subtropical origin was clearly identifiable
382 at station 26 by the steep gradient of the isotherms and isohalines between station 26 and 29; salinity dropping
383 from 35.34 psu to 35.01 psu (Figure 2). North of the Sub-Arctic Front, LSW and ISOW display high
384 PFe/PAI ratios, ranging from 0.36 to 0.44 mol mol⁻¹. These high ratios, compared to the crustal one, could be
385 associated to higher content of PFe from biogenic origin, especially in the case of the LSW.

386 While the Iceland, Irminger and the Labrador basins are characterised with median %PFe value under 55%. An
387 interesting feature observable was the dramatic decrease of the %PFe proxy values happening at the station 26

Field Code Changed

Formatted: English (United Kingdom)

Formatted: English (United Kingdom)

388 (Figure 6). This feature is likely be associated to the presence of the Sub-Arctic Front, located between 49.5 and
389 51°N latitude and 23.5 and 22°W longitude (Zunino et al., 2017). Indeed, this front which separates cold and
390 fresh water of subpolar origin from warm and salty water of subtropical origin was clearly identifiable at station
391 26 by the steep gradient of the isotherms and isohalines (Figure 2).

392 4.2. Fingerprinting water masses

393
394
395 The GEOVIDE section crossed several distinct water masses along the North Atlantic. Based on , each of them
396 being distinguishable by their salinity and potential temperature signatures (García Ibáñez et al., 2015; Figure
397 2). Based on this study, we applied a Kruskal-Wallis test on molar PFe/PAI ratios of nine water masses (Figure
398 7) in order to test the presence of significant differences. Water masses for which we had less than 5 data
399 points for PFe/PAI were excluded from this test. As the differences in the median values among the treatment
400 groups were greater than would be expected by chance; the difference in PFe/PAI between water masses is
401 statistically significant ($P < 0.001$).

402 As previously seen, the lithogenic imprint is dominant in the WEB, with MW and NEADW showing PFe/PAI
403 values close to the UCC value of $0.21 \text{ mol mol}^{-1}$. Interestingly, the PFe/PAI signature of $0.36 \text{ mol mol}^{-1}$ within
404 the old LSW_{WEB} is probably due to the effect of biogenic inputs associated with the strong bloom encountered in
405 the Irminger Sea than in the WEB (see section 4.3.5). While it appears that lithogenic particles are dominating
406 the water column in the FWEB and that some water masses have a clear PFe/PAI fingerprint, it is important to
407 discuss the origin of these signatures, which is the purpose of the following sections.

410 4.2.3. Tracking the different inputs of particulate iron

411 4.2.3.1. Inputs at margins: Iberian, Greenland and Newfoundland

412 Inputs from continental shelves and margins have been demonstrated to support high productivity in shallow
413 coastal areas. Inputs of iron from continental margin sediments supporting the high productivity found in
414 shallow coastal regions have been demonstrated in the past (e.g. Cullen et al. (2009), Elrod et al. (2004), Jeandel
415 et al. (2011), Ussher et al. (2007)) and sometimes, were shown to be advected at great distances from the coast
416 (e.g. Lam and Bishop et al., 2008).

417 In the following section, we will investigate these possible candidate sources in proximity of the different
418 margins encountered. Along the GEOVIDE section, sediments at margins were of various compositions
419 (Dutkiewicz et al., 2015). Sediments originating from the Iberian margin were mainly constituted of silts and
420 clays (Caeador et al., 1996; Duarte et al., 2014). East Greenland margin sediments were a mixture of sands and
421 grey/green muds, while, sediments from the West Greenland margin were mainly composed of grey/green muds
422 (Loring and Asmund, 1996). At the western end of the section, sediments from the Newfoundland margin were
423 composed of gravelly and sandy muds (Mudie et al., 1984). The different sediment compositions of the three
424 margins sampled during GEOVIDE have different mineralogy/composition, which are reflected in their

425 different PFe/PAI ratios (Figure 8). While the Iberian Margin had a PFe/PAI close to UCC ratio, the highest
426 ratio could be seen at the East Greenland (stations 53 and 56) and West Greenland (station 61) Margins, with
427 median PFe/PAI reaching 0.45 mol·mol⁻¹. The Newfoundland margin displayed an intermediate behaviour, with
428 Fe/Al ratios of 0.35 mol·mol⁻¹.

429 In addition to PAI, PMn can be used as a tracer of inputs from shelf resuspension (Lam and Bishop, 2008).
430 Indeed, Mn is really sensitive to oxidation mediated by bacteria (Tebo et al., 1984; Tebo and Emerson, 1985)
431 and forms manganese oxides (MnO₂). These authigenic particles lead to an enrichment of Mn in particle
432 compositions. In order to track the influence of shelf resuspension, a percentage of sedimentary inputs “%bulk
433 sediment inputs” can be estimated using PMn/PAI ratio from GEOVIDE samples and the PMn/PAI UCC value
434 (0.0034; Taylor and McLennan, 1995) according to the following equation:

$$\% \text{bulk sediment PMn} = 100 * \left(\frac{\text{PAI}}{\text{PMn}} \right)_{\text{sample}} * \left(\frac{\text{PMn}}{\text{PAI}} \right)_{\text{UCC ratio}} \quad (3)$$

436 This proxy is a good indicator of direct and recent sediment resuspension. We assume that particles newly
437 resuspended in water column will have the same PMn/PAI ratio than the UCC ratio leading to a “%bulk
438 sediment Mn” of 100%. This value will decrease by authigenic formation of Mn oxides. This proxy assumes
439 homogeneity of the sediment PMn/PAI ratio through the section which is maybe not completely the case at
440 every station. In consequence, this proxy is only a tool to identify new benthic resuspension at specific location
441 and inter-comparison between several locations is not possible. When a sample presents a “%bulk sediment
442 Mn” greater than 100%, we assign a value of 100% to simplify the following discussion. As the Mn cycle can
443 also be affected by biologic uptake (e.g. Peers and Price, 2004; Sunda and Huntsman, 1983), this proxy is only
444 used at depths where biologic activity is negligible (i.e. below 150m depth).

445 *The Iberian margin*

446 The Iberian margin was an important source of lithogenic-derived iron-rich particles in the Atlantic Ocean
447 during GEOVIDE: shelf resuspension impact was perceptible until 280 km away from the margin (Station 11)
448 in the Iberian Abyssal Plain (Figure 8).

449 On the shelf, at station 2 high sediment resuspension was observable by low beam transmissometry value
450 (87.6%) at the immediate vicinity of the seafloor (153m). This sediment resuspension led to an extensive input
451 of lithogenic particles within the water column associated with high concentrations of PFe (304 nmol L⁻¹), PAI
452 (1500 nmol L⁻¹), and PMn (2.5 nmol L⁻¹) (Figure 3, Table S1). Moreover, one hundred percent 100% of PFe
453 is was estimated to have a lithogenic origin (Figure 8) while 100% of the PMn was estimated to be the result
454 of a recent sediment resuspension according to the %Fe_{litho} and “%bulk sediment Mn” proxies (supplementary
455 material, Table S2 Figure 8), confirming the resuspended particle input.

456 Coastal waters of the Iberian Shelf are impacted by the runoff for the Tagus River, which is characterised by
457 high suspended matter discharges, ranging between 0.4 to 1 × 10⁶ tons·yr⁻¹, and with a high anthropogenic
458 signature (Jouanneau et al., 1998). During the GEOVIDE section, the freshwater input was observable at
459 stations 1, 2 and 4 in the first 20 m; salinity was below 35.2 psu while surrounding waters masses had salinity
460 up to 35.7 psu. Within the freshwater plume, particulate concentrations were important at station 2 with PFe of
461 up to 35.7 psu. Within the freshwater plume, particulate concentrations were important at station 2 with PFe of
462 up to 35.7 psu.

463 1.83 nmol L⁻¹. Further away from the coast, the particulate concentrations remained low at 20m depth, with PFe,
464 PAI, and PMn concentrations of 0.77 nmol L⁻¹, 3.5 nmol L⁻¹, and 0.04 nmol L⁻¹, respectively at station 1. The
465 low expansion of the Tagus plume is likely due to the rapid settling of suspended matter. Indeed, our coastal
466 station 2 was already located at around 50 km of the Iberian coast and according to Jouanneau et al. (1998), the
467 surface particle load can be observable at a maximum 30km of the Tagus estuary.

468 Besides, ADCP data acquired during GEOVIDE (Zunino et al., 2017) and several studies have reported an
469 intense current spreading northward coming from Strait of Gibraltar and Mediterranean Sea, leading to a strong
470 resuspension of benthic sediments above the Iberian Shelf, e.g. Biscaye and Eittrheim (1977), Eittrheim et al.
471 (1976), McCave and Hall (2002), Spinrad et al. (1983). ~~The importance of the sediment resuspension was~~
472 ~~observable by low beam transmissometry value (87.6%) at the bottom of station 2. This important sediment~~
473 ~~resuspension led to an extensive input of lithogenic particles within the water column associated with high~~
474 ~~concentrations of PFe (304 nmol L⁻¹), PAI (1500 nmol L⁻¹), and PMn (2.5 nmol L⁻¹) (Figure 3, Table S1).~~

475 Moreover, one hundred percent of PFe is estimated to have a lithogenic origin (Figure 10) while 100% of the
476 PMn was estimated to be the result of a recent sediment resuspension according to the %Fe_{litho} and %bulk
477 sediment Mn²⁺ proxies (supplementary material, Table S2), confirming the resuspended particle input.

478 At distance from the shelf, within the Iberian Abyssal Plain, an important lateral advection of PFe from the
479 margin was observable (Figure 108). These lateral inputs occurred at two depth ranges: between 400 and 1000
480 m as seen at stations 4 and 1, with PFe concentrations reaching 4 nmol L⁻¹, and between 2500 m and the bottom
481 (3575 m) of station 1, with PFe concentrations reaching 3.5 nmol L⁻¹. While 100% of PFe had a lithogenic
482 signature, the sedimentary source input estimation decreased, between 40% and 90% of the PMn (Figure 108).
483 Transport of lithogenic particles was observable until station 11 (12.2°W) at 2500 m where PFe concentration
484 was 7.74 nmol L⁻¹ and 60% of PMn had a sedimentary origin (Figure 49). Noteworthy, no particular increase in
485 PFe, PMn or PAI was seen between 500 and 2000 m depth, where the MOW spreads, which is consistent with
486 that was observed DFe concentrations (Tonnard et al., this issue); yet in contrast with the dissolved aluminium
487 values (Menzel-Barraqueta et al., ~~subm.2018~~, this issue) which were high in the MOW and with the study of
488 Ohnemus and Lam (2015) that reported a maximum PFe concentration at 695 m depth associated with the
489 particle-rich Mediterranean Overflow Water (Eittrheim et al., 1976) in the IAP. However, their station was
490 located further south of our station 1. The shallower inputs observed at stations 1 and 4 could therefore be
491 attributed to sediment resuspension from the Iberian margin and nepheloid layer at depth for station 1.

492
493 Surface coastal waters of the Iberian Shelf are impacted by the runoff for the Tagus River, which is
494 characterised by high suspended matter discharges, ranging between 0.4 to 1 × 10⁶ tons yr⁻¹, and with a high
495 anthropogenic signature (Jouanneau et al., 1998). During the GEOVIDE section, the freshwater input was
496 observable at stations 1, 2 and 4 in the first 20 m; salinity was below 35.2 psu while surrounding waters masses
497 had salinity up to 35.7 psu. Within the freshwater plume, particulate concentrations were high at station 2 with
498 PFe of 1.83 nmol L⁻¹. Further away from the coast, the particulate concentrations remained low at 20m depth,
499 with PFe, PAI, and PMn concentrations of 0.77 nmol L⁻¹, 3.5 nmol L⁻¹, and 0.04 nmol L⁻¹, respectively at station
500 1. The low expansion of the Tagus plume is likely due to the rapid settling of suspended matter. Indeed, our
501 coastal station 2 was already located at around 50 km of the Iberian coast and according to Jouanneau et al.

Formatted: Space After: 10 pt

Formatted: Space After: 10 pt

502 (1998), the surface particle load can be observable at a maximum 30km of the Tagus estuary. Overall, the
503 Iberian margin appears to be an important source of lithogenic-derived iron rich particles in the Atlantic Ocean.
504 Therefore, the Iberian margin appears to be an important source of lithogenic-derived iron-rich particles in the
505 Atlantic Ocean; shelf resuspension impact was perceptible until 280 km away from the margin (Station 11) in
506 the Iberian Abyssal Plain.

507

508 *South Greenland*

509 Several studies already demonstrated the importance of icebergs and sea ice as source of dissolved and
510 particulate iron (e.g. van der Merwe et al., 2011a, 2011b; Planquette et al., 2011; Raiswell et al., 2008). The
511 Greenland shelf is highly affected by external fresh water inputs as ice melting or riverine runoff (Fragoso et al.,
512 2016), that are important sources of iron to the Greenland Shelf (Bhatia et al., 2013; Hawkings et al., 2014;
513 Statham et al., 2008). Along GEOVIDE, Greenland shelves were a source of particulate-rich meteoric water
514 leading to a transfer of DFe to PFe by an enhanced biological activity. Indeed,

515 ~~Both~~ East and West Greenland shelves (stations 53 and 60) had high concentration of particles (beam
516 transmissometry of 83%) and particulate trace elements, reaching 22.1 nmol L⁻¹ and 18.7 nmol L⁻¹ of PFe,
517 respectively (station 53 at 100m and station 61 at 136 m). Several studies already demonstrated the importance
518 of icebergs and sea ice melting as sources of dissolved and particulate iron (e.g. van der Merwe et al., 2011a,
519 2011b; Planquette et al., 2011; Raiswell et al., 2008). The Greenland shelf is highly affected by external fresh
520 water inputs such as sea-ice-melting or riverine runoff (Fragoso et al., 2016), that are important sources of iron
521 to the Greenland Shelf (Bhatia et al., 2013; Hawkings et al., 2014; Statham et al., 2008).

522 During the cruise, the relative freshwater observed (S<33 psu) within the first 25 meters of stations 53 and 61
523 were associated with high PFe (19 nmol L⁻¹), PAI (61 nmol L⁻¹), PMn (0.6 nmol L⁻¹) and a low beam
524 transmissometry (≤ 85%) (Figure 94 and Table S1). Particles associated were enriched in iron compared to
525 aluminium, as PFe/PAI ratio was 0.3 within the meteoric water plume. High biological production, in agreement
526 with PP concentrations reaching 197 nmol L⁻¹ induced by the supply of bioavailable dissolved iron from
527 meteoric water (Raiswell et al., 2008; Statham et al., 2008; Tonnard et al., submitted, this issue), led to a
528 transfer of DFe to the particulate phase. This is in line with the fact that around 30% PFe had a non-lithogenic
529 origin. In addition, only 40% PMn originated from resuspended sediments. Interestingly, these two proxies
530 remained constant from the seafloor to the surface (Station 49, Figure 108), with around 25% of the PMn of
531 sedimentary origin, which could be due to an important mixing happening on the shelf. The lithogenic PFe
532 could result from the release of PFe from Greenland bedrock captured during the ice sheet formation on land.

533 The spatial extent of the off-shelf lateral transport of particles was not important on the east Greenland coast.
534 Indeed, no visible increase of particulate trace metal concentrations was visible at the first station off-shelf,
535 station 60 (Figure 108), except at 1000 m depth, where a strong increase (up to 90%) of sedimentary PMn was
536 seen. This is probably due to the East Greenland Coastal Current (EGCC) that was located at station 53
537 constrained these inputs while stations 56 and 60 were under the influence of another strong current, the East
538 Greenland-Irminger current (EGIC) (Zunino et al., 2017).

539 To the west of the Greenland margin, lateral transport of particles was slightly more important. Noticeable
540 concentrations of particulate lithogenic elements were observable until station 64 located 125 km away from
541 shoreline. These particles had decreasing PFe lithogenic contribution (50%) with a similar (25%) sedimentary

542 PMn content than closer to the margin. The increasing nature of non-lithogenic PFe is linked to the bloom in
543 surface (associated with a PFe/PAI ratio of 0.30 mol mol⁻¹, a PP of 197 nmol L⁻¹ at station 61 and a ~~Chl-a~~
544 ~~concentrations of 6.21 mgChl-a concentration of 6.21 mg m⁻³~~), with the biogenic PFe settling down along the
545 transport of particles.

546 ~~Therefore, particles newly resuspended from Greenland sediments are an important source, representing around~~
547 ~~one a third of the pMn pool, combined with surface inputs such as riverine runoff and/or ice-melting that are~~
548 ~~delivering particles on the shelf and biological production. Unlike the Iberian shelf, Greenland margin was not~~
549 ~~an important provider of particulate metals inside the Irminger and Labrador Basin, due to the circulation that~~
550 ~~constrained the extent of the margin plume.~~

551
552 ~~Therefore, particles newly resuspended from Greenland sediments are an important source, representing around~~
553 ~~a third of the pMn pool, combined with surface inputs such as riverine runoff and/or ice-melting that are~~
554 ~~delivering particles on the shelf and biological production. Unlike the Iberian shelf, Greenland margin was not~~
555 ~~an important provider of particulate metals inside the Irminger and Labrador Basin, due to the circulation that~~
556 ~~constrained the extent of the margin plume.~~

557
558 *The Newfoundland Shelf*

559 Previous studies already described the influence of fresh water on the Newfoundland shelf from the Hudson
560 Strait and/or Canadian Arctic Archipelago (Fragoso et al., 2016; Yashayaev, 2007). Yashayaev (2007) also
561 monitored strong resuspension of sediments associated with the spreading of Labrador Current along the West
562 Labrador margin.

563 Close to the Newfoundland coastline, at station 78, high fresh water discharge (≤ 32 psu) was observed in
564 surface (Benetti et al., 2017). Interestingly, these freshwater signatures were not associated with elevated
565 particulate trace metal concentrations. Distance of meteoric water sources implied a long travel time for the
566 water to spread through the Labrador Basin to our sampling stations. Along the journey, particles present
567 originally may have been removed from water column by gravitational settling.

568 The proportion of lithogenic PFe was relatively high and constant in the entire water column, with a median
569 value of 70%. At station 78, 100% of the PMn had a sedimentary origin close to the seafloor (371 m). The
570 spreading of the recent sediment resuspension was observable until 140 m depth where the contribution of
571 sedimentary Mn was still 51% (Figure 408, Table S2). This could correspond to an intense nepheloid layer as
572 previously reported by Biscaye and Eitrem (1977) (see also section 3.3.2). The high PFe concentration (184
573 nmol L⁻¹, station 78, 371 m) associated with a high percentage of sedimentary PMn (95%) observed at the
574 bottom of this station, was therefore the result of an important resuspension of shelf sediments. This was
575 confirmed with low transmissometry values of 95%.

576 The important phytoplanktonic community present (maximum Chl-a= 4.91 mg m⁻³, Tonnard et al., in prep), is
577 linked to low PFe of 0.79 nmol L⁻¹ at 10 m, but, with a high PFe/PAI ratio, up to 0.4, and PP concentration of 97
578 nmol L⁻¹, confirming the biologic influence. Either the biogenic particles settled quickly, and/or they were
579 quickly remineralized. Concerning this latter process, intense remineralization at station 77 (7 mmol C m⁻² d⁻¹
580 compared to 4 mmol C m⁻² d⁻¹ in the Western European Basin) has been reported by Lemaitre et al. (2018a and
581 2018b), which could explain the low PFe values throughout the water column.

582

583 Along the GEOVIDE section, continental shelves provided an important load of particles within the surrounding
584 water column. The three margins sampled during GEOVIDE behaved differently; the Iberian margin discharged
585 high quantities of lithogenic particles far away from the coast while the Greenland and Newfoundland margins
586 did not reveal important PFe concentrations. Spreading of particles is tightly linked to hydrodynamic conditions,
587 which in the case of the Greenland margin, prevented long distance seeding of PFe. Moreover, each margin
588 showed a specific PFe/PAI ratio (Figure 8) indicating different composition of the resuspended particles.
589 Resuspended particles represent the composition of sediment at the margin if oxido-reductive transformation of
590 iron and aluminium are considered negligible under these circumstances. Differences between margins were due
591 to the presence of non-crustal particles, either biogenic or authigenic. Biological production in surface waters
592 and authigenic formation of iron hydroxide produce particles with a higher PFe/PAI content and their export
593 through the water column to the sediment increased the PFe/PAI ratio at depth. Regions where biological
594 production is intense such as in the vicinity of Newfoundland presented higher PFe/PAI ratios of resuspended
595 benthic particles.

596 Along the GEOVIDE section, continental shelves provided an important load of particles within the surrounding
597 water column. The three margins sampled during GEOVIDE behaved differently; the Iberian margin discharged
598 high quantities of lithogenic particles far away from the coast while the Greenland and Newfoundland margins
599 did not reveal important PFe concentrations. Spreading of particles is tightly linked to hydrodynamic conditions,
600 which in the case of the Greenland margin, prevented long distance seeding of PFe. Moreover, each margin
601 showed a specific PFe/PAI ratio (Figure 98) indicating different composition of the resuspended particles.
602 Resuspended particles represent the composition of sediment at the margin if oxido-reductive **redox**
603 transformation of iron and aluminium are considered negligible under these circumstances. Differences between
604 margins were due to the presence of non-crustal particles, either biogenic or authigenic. Biological production in
605 surface waters and authigenic formation of iron hydroxide produce particles with a higher PFe/PAI content and
606 their export through the water column to the sediment increased the PFe/PAI ratio at depth. Regions where
607 biological production is intense such as in the vicinity of Newfoundland presented higher PFe/PAI ratios of
608 resuspended benthic particles.

609

610

4.23.2 Benthic resuspended sediments

611 Along the GEOVIDE section, **Benthic nepheloid layers (BNLs)** BNLs are providing high concentrations of
612 particulate trace element in the deep open ocean, contributing highly to the total trace elements budget as iron.

613 **Along the GA01 section, BNLs were observable in each province with different strengths (Figures 3 and 120).**

614 **Benthic nepheloid layers (BNLs) are important layers where local resuspension of sedimentary particles (Bishop**
615 **and Biscaye, 1982; Eittrheim et al., 1976; Rutgers Van Der Loeff et al., 2002) occur due to strong hydrographic**
616 **stresses (i.e. boundary currents, benthic storms and deep eddies) interacting with the ocean floor (Biscaye and**
617 **Eittrheim, 1977; Eittrheim et al., 1976; Gardner et al., 2017, 2018). Along the GA01 section, BNLs were**
618 **observable in each province with different strengths (Figures 3 and 12).**

619 In BNLs located within the WEB, PFe concentrations reached up to 10 nmol L⁻¹ (stations 26 and 29, Table S1).

620 These concentrations were smaller than PFe concentrations encountered in BNL from the Icelandic (**stations 32**

621 **and 34), Irminger (stations 42 and 44) and Labrador Basins (stations 68, 69 and 71), where benthic resuspension**

622 led to PFe concentrations higher than 40 nmol L⁻¹, even reaching 89 nmol L⁻¹ at the bottom of station 71 (3736
623 m). Moreover, in the Irminger and Labrador Basins, PFe/PAI molar ratios within BNLs were higher than the
624 ones measured within the WEB at station 26 and 29. In the Irminger Basin, PFe/PAI reached 0.4 mol mol⁻¹
625 (Figure 10), which could reveal a mixture of lithogenic and biogenic matter previously exported. This feature
626 was also observed in the Labrador Basin, with PFe/PAI ratio ranging between 0.34 and 0.44 mol mol⁻¹. In
627 contrast, BNLs sampled in the WEB have clearly a lithogenic imprint, with PFe/PAI molar ratios close to the
628 crustal one. Resuspended sediments with a non-crustal contribution seem to hold a higher PFe content than
629 sediments with a lithogenic characteristic. Nevertheless, interestingly all BNLs present during GEOVIDE were
630 spreading identically, with impacts observable up to 200 meters above the oceanic seafloor (Figure 10), as
631 reflected in beam transmissometry values, and PFe concentrations, that returned to a background level at 200 m
632 above the seafloor. The presence of these BNLs has also been reported by Le Roy et al. (submitted, this issue)
633 using radium-226 activity. Important differences of PFe intensities could also be due to different hydrographic
634 components and topographic characteristics. BNLs are occurring due to strong hydrographic stresses (i.e.
635 boundary currents, benthic storms and deep eddies) interacting with the ocean floor (Biscaye and Eittrheim, 1977;
636 Eittrheim et al., 1976; Gardner et al., 2017, 2018). They are As previously explained, two main triggers of BNLs
637 are benthic storms and deep eddies; by definition these processes are highly variable geographically and
638 temporally, but no physical data could allow us to investigate further this hypothesis.
639 Benthic nepheloid layers (BNLs) are important layers where local resuspension of sedimentary particles (Bishop
640 and Biscaye, 1982; Eittrheim et al., 1976; Rutgers Van Der Loeff et al., 2002) occur due to strong hydrographic
641 stresses (i.e. boundary currents, benthic storms and deep eddies) interacting with the ocean floor (Biscaye and
642 Eittrheim, 1977; Eittrheim et al., 1976; Gardner et al., 2017, 2018). Along the GA01 section, BNLs were
643 observable in each province with different strengths (Figures 3 and 12).
644 Along the GEOVIDE section, BNLs are providing high concentrations of particulate trace element in the deep
645 open ocean, contributing highly to the total trace elements budget as iron.

647 4.23.3. Reykjanes Ridge inputs

648 Above the ridge, high PFe concentrations were measured, reaching 16 nmol L⁻¹ just above the seafloor, while
649 increased DFe concentrations were reported to the East of the ridge (Tonnard et al., this issue). The exact
650 sources of iron-rich particles cannot be well constrained, as they could come from active hydrothermal vents or
651 resuspension of particulate matter from new crustal matter produced at the ridge. According to the oceanic
652 circulation (Zunino et al., 2017; Garcia-Ibanez et al., 2017), hydrothermal particles could have been seen in the
653 ISOW within the Icelandic Basin. Nevertheless, at the vicinity of the ridge, scanning electron microscope
654 (SEM) analyses of our samples did reveal a number of biological debris and clays but not the presence of iron
655 (oxy-)hydroxide particles (supplementary figure S1), which are known to be highly produced close to
656 hydrothermal vents (Elderfield and Schultz, 1996). Their absence could thus indicate an absence of vents.
657 However, other proxies, such as helium-3, are necessary to claim with more accuracy the presence or absence of
658 an hydrothermal source close to station 38.

660 4.32.4. Atmospheric inputs

661 Atmospheric deposition is an important input of trace elements in surface of the open ocean (e.g. (Jickells et al.,
662 2005). Atmospheric inputs, both wet and dry, were reported to be low during the GEOVIDE cruise (Menzel-
663 Barraqueta et al., 2018, this issue; Shelley et al., 2017; 2018). In fact, oceanic particles measurements in
664 surface waters along the section did not reveal high PFe or PAI ~~concentrations, concentrations. therefore, the~~
665 ~~surface composition of particles did not seem to be highly affected by atmospheric deposition at the time of the~~
666 ~~cruise.~~ One pattern is ~~also~~ interesting to note: the surface waters of the Iberian Abyssal Plain and Western
667 European Basin, between stations 11 and 23 presented a characteristic feature with really low PFe/PAI
668 elemental ratios, of 0.11, smaller than the UCC ratio of 0.21 (Figure 6). Such low ratios have been reported in
669 the same region by Barrett et al. (2012). One possible explanation is given by Buck et al. (2010) who described
670 Fe-depleted aerosols in this area of the North Atlantic with PFe/PAI ratio below UCC ratio. However, Shelley et
671 al. (2017) found a higher PFe/PAI ratio around 0.25 in this area (their sample geoa5-6). This result, highlights
672 some of the difficulties that link atmospheric inputs to water column data (Baker et al., 2016), and implies a
673 probable fractionation after aerosol deposition. In addition, there is high spatial and temporal variability of
674 atmospheric deposition (Mahowald et al., 2005) and a certain degree of uncertainty about the dissolution
675 processes of atmospherically-transported particles (Bonnet and Guieu, 2004).

676
677

678 5. Conclusions

679

680 The investigation of the PFe compositions of suspended particulate matter along the GEOVIDE section in the
681 North Atlantic reflects the pervasive influence of crustal particles, augmented by sedimentary inputs at margins,
682 and within benthic nepheloid layers at depths. In consequence, variance of particulate iron along the section is
683 mainly explained by lithogenic factors.

684 Resuspension of sedimentary particles from continental shelves are responsible of high particulate iron
685 concentration within the surrounding water column, and could be observed at long distances, in the case of the
686 Iberian margin. Due to the hydrodynamics conditions, lithogenic particles are exported off shore up to 280 km
687 away off the Iberian margin. Our results also demonstrate the impact of arctic meteoric water in the
688 biogeochemical cycle of trace elements on the Greenland shelf while in surface, the enhancement of
689 productivity by new bioavailable iron is leading to a transfer of dissolved iron to the particulate phase.

690 Above the Reykjanes Ridge, resuspension of particles were responsible of the PFe enrichment of the Iceland
691 Scottish Overflow Water.

692 Our dataset allowed the investigation of scavenging processes that were sometimes visible at depths greater than
693 1000m, these effects being the most pronounced within the WEB.

694 Overall, particulate iron distribution in the North Atlantic is strongly affected by sources at its boundaries. This
695 work, within the frame of the GEOTRACES program, will allow a better understanding of the cycle of
696 particulate iron, when combined to other datasets in a modelling exercise for example.

697

698 ~~This investigation of the PFe compositions of suspended particulate matter along the GEOVIDE section in the~~
699 ~~North Atlantic indicates reflects the pervasive influence of crustal particles, augmented by sedimentary inputs at~~
700 ~~margins, and at depths, within benthic nepheloid layers. Rary particles are responsible of high concentration. In~~

Formatted: Justified, Line spacing: 1.5 lines, No widow/orphan control, Don't adjust space between Latin and Asian text, Don't adjust space between Asian text and

Formatted: Font: Times New Roman, English (United Kingdom)

Formatted: Font: (Default) Helvetica, 11 pt, Font color: Auto

701 ~~particular, hallowed the export of while in surface, twill il faudrait une phrase d'ouverture plutôt~~
702 ~~Indeed, along the GEOVIDE section, continental shelves provided an important load of particles within the~~
703 ~~surrounding water column, with PFe mostly residing in non-biogenic particulate form. The Iberian margin~~
704 ~~discharged high quantities of lithogenic particles originating from riverine inputs far away from the coast while~~
705 ~~the Greenland margin did not reveal a long distance seeding of PFe, due to hydrodynamic conditions. Both~~
706 ~~Greenland and Newfoundland margins PFe resuspended particles were under a strong biogenic influence that~~
707 ~~were exported at depth. This resulted in different remineralisation fluxes among the different provinces.~~
708 ~~Seavenging processes could also be visible at depths greater than 1000 m, these effects being the most~~
709 ~~pronounced within the Labrador Basin.~~
710 ~~Finally, resuspended sediments above the Reykjanes Ridge increased the PFe composition of the Iceland~~
711 ~~Scottish Overflow Water. A similar feature occurs for the Labrador Sea Water, as it flows from the Irminger~~
712 ~~Basin to the Western European Basin.~~

713

714

715

716 **Acknowledgments**

717 We are greatly indebted to the captain and crew of the N/O Pourquoi Pas? for their help during the GEOVIDE
718 mission and clean rosette deployment. We would like to give special thanks to Fabien Pérault and Emmanuel de
719 Saint Léger for their technical expertise, to Catherine Schmechtig for the GEOVIDE database management and
720 Greg Cutter for his guidance in setting up the new French clean sampling system. We also would like to thanks
721 Reiner Schlitzer for the Ocean Data View software (ODV).

722 This work was supported by the French National Research Agency (ANR-13-BS06-0014, ANR-12-PDOC-
723 0025-01), the French National Centre for Scientific Research (CNRS-LEFE-CYBER), the LabexMER (ANR-
724 10-LABX-19), and Ifremer. It was supported for the logistic by DT-INSU and GENAVIR.

725

726 **References**

727

728 Aguilar-Islas, A. M., Rember, R., Nishino, S., Kikuchi, T. and Itoh, M.: Partitioning and lateral transport of iron
729 to the Canada Basin, *Polar Sci.*, 7(2), 82–99, doi:10.1016/j.polar.2012.11.001, 2013.

730 Baker, A. R., Adams, C., Bell, T. G., Jickells, T. D. and Ganzeveld, L.: Estimation of atmospheric nutrient
731 inputs to the Atlantic Ocean from 50°N to 50°S based on large-scale field sampling: Iron and other dust-
732 associated elements, *Global Biogeochem. Cycles*, 27(3), 755–767, doi:10.1002/gbc.20062, 2013.

733 Baker, A. R., Landing, W. M., Bucciarelli, E., Cheize, M., Fietz, S., Hayes, C. T., Kadko, D., Morton, P. L.,
734 Rogan, N., Sarthou, G., Shelley, R. U., Shi, Z., Shiller, A. and van Hulten, M. M. P.: Trace element and isotope
735 deposition across the air–sea interface: progress and research needs, *Philos. Trans. R. Soc. A Math. Phys. Eng.*
736 *Sci.*, 374(2081), 20160190, doi:10.1098/rsta.2016.0190, 2016.

737 Barrett, P. M., Resing, J. A., Buck, N. J., Buck, C. S., Landing, W. M. and Measures, C. I.: The trace element
738 composition of suspended particulate matter in the upper 1000m of the eastern North Atlantic Ocean: A16N,
739 Mar. Chem., 142–144, 41–53, doi:10.1016/j.marchem.2012.07.006, 2012.

740 ~~Benetti, M., Reverdin, G., Lique, C., Yashayev, I., Holliday, N. P., Tynan, E., Torres-Valdes, S., Lherminier,~~
741 ~~P., Tréguer, P., and Sarthou, G.: Composition of freshwater in the spring of 2014 on the southern Labrador shelf~~
742 ~~and slope, Journal of Geophysical Research: Oceans, 122, 1102-1121, 10.1002/2016jc012244, 2017.~~

743

744 Berger, C. J. M., Lippiatt, S. M., Lawrence, M. G. and Bruland, K. W.: Application of a chemical leach
745 technique for estimating labile particulate aluminum, iron, and manganese in the Columbia River plume and
746 coastal waters off Oregon and Washington, J. Geophys. Res., 113, C00B01, doi:10.1029/2007JC004703, 2008.

747 Bergquist, B. A., Wu, J. and Boyle, E. A.: Variability in oceanic dissolved iron is dominated by the colloidal
748 fraction, Geochim. Cosmochim. Acta, 71(12), 2960–2974, doi:10.1016/j.gca.2007.03.013, 2007.

749 Bhatia, M. P., Kujawinski, E. B., Das, S. B., Breier, C. F., Henderson, P. B. and Charette, M. A.: Greenland
750 meltwater as a significant and potentially bioavailable source of iron to the ocean, Nat. Geosci., 6(4), 274–278,
751 doi:10.1038/ngeo1746, 2013.

752 Biscaye, P. E. and Eitrem, S. L.: Suspended Particulate Loads and Transports in the Nepheloid Layer of the
753 Abyssal Atlantic Ocean, Dev. Sedimentol., 23(C), 155–172, doi:10.1016/S0070-4571(08)70556-9, 1977.

754 Bishop, J. K. B. and Biscaye, P. E.: Chemical characterization of individual particles from the nepheloid layer in
755 the Atlantic Ocean, Earth Planet. Sci. Lett., 58(2), 265–275, doi:10.1016/0012-821X(82)90199-6, 1982.

756 Bishop, J. K. B. and Fleisher, M. Q.: Particulate manganese dynamics in Gulf Stream warm-core rings and
757 surrounding waters of the N.W. Atlantic, Geochim. Cosmochim. Acta, 51(10), 2807–2825, doi:10.1016/0016-
758 7037(87)90160-8, 1987.

759 Bonnet, S. and Guieu C.: Dissolution of atmospheric iron in seawater, Geophys. Res. Lett., 31(3), L03303,
760 doi:10.1029/2003GL018423, 2004.

761 Boyle, E. A., Bergquist, B. A., Kayser, R. A. and Mahowald, N.: Iron, manganese, and lead at Hawaii Ocean
762 Time-series station ALOHA: Temporal variability and an intermediate water hydrothermal plume, Geochim.
763 Cosmochim. Acta, 69(4), 933–952, doi:10.1016/j.gca.2004.07.034, 2005.

764 Buck, C. S., Landing, W. M., Resing, J. A. and Measures, C. I.: The solubility and deposition of aerosol Fe and
765 other trace elements in the North Atlantic Ocean: Observations from the A16N CLIVAR/CO2repeat
766 hydrography section, Mar. Chem., 120(1–4), 57–70, doi:10.1016/j.marchem.2008.08.003, 2010.

767 ~~Cacador, I., Vale, C. and Catarino, F.: The influence of plants on concentration and fractionation of Zn, Pb, and~~
768 ~~Cu in salt marsh sediments (Tagus Estuary, Portugal), J. Aquat. Ecosyst. Heal., 5(3), 193–198,~~

769 [doi:10.1007/BF00124106](https://doi.org/10.1007/BF00124106), 1996. Cheize, M., Planquette, H. F., Fitzsimmons, J. N., Pelleter, E., Sherrell, R. M.,
770 Lambert, C., Bucciarelli, E., Sarthou, G., Le Goff, M., Liorzou, C., Chéron, S., Viollier, E., and Gayet, N.:
771 [Contribution of resuspended sedimentary particles to dissolved iron and manganese in the ocean: An
772 experimental study, *Chemical Geology*. doi: 10.1016/j.chemgeo.2018.10.003, 2018.](https://doi.org/10.1016/j.chemgeo.2018.10.003)

773 Collier, R. and Edmond, J.: The trace element geochemistry of marine biogenic particulate matter, *Prog.*
774 *Oceanogr.*, 13(2), 113–199, doi:10.1016/0079-6611(84)90008-9, 1984.

775 Cullen, J. T., Chong, M. and Janson, D.: British columbian continental shelf as a source of dissolved iron to the
776 subarctic northeast Pacific Ocean, *Global Biogeochem. Cycles*, 23(4), 1–12, doi:10.1029/2008GB003326, 2009.

777 Cutter, G. A. and Bruland, K. W.: Rapid and noncontaminating sampling system for trace elements in global
778 ocean surveys, *Limnol. Oceanogr. Methods*, 10(JUNE), 425–436, doi:10.4319/lom.2012.10.425, 2012.

779 Damshäuser, A., Wagener, T., Garbe-Schönberg, D. and Croot, P.: Particulate and dissolved aluminum and
780 titanium in the upper water column of the Atlantic Ocean, *Deep. Res. Part I Oceanogr. Res. Pap.*, 73, 127–139,
781 doi:10.1016/j.dsr.2012.12.002, 2013.

782 Dehairs, F., Jacquet, S., Savoye, N., Van Mooy, B. A. S., Buesseler, K. O., Bishop, J. K. B., Lamborg, C. H.,
783 Elskens, M., Baeyens, W., Boyd, P. W., Casciotti, K. L. and Monnin, C.: Barium in twilight zone suspended
784 matter as a potential proxy for particulate organic carbon remineralization: Results for the North Pacific, *Deep.*
785 *Res. Part II Top. Stud. Oceanogr.*, 55(14–15), 1673–1683, doi:10.1016/j.dsr2.2008.04.020, 2008.

786 [Duarte, B., Silva, G., Costa, J. L., Medeiros, J. P., Azeda, C., Sá, E., Metelo, I., Costa, M. J. and Caçador, I.:
787 Heavy-metal distribution and partitioning in the vicinity of the discharge areas of Lisbon drainage basins \(Tagus
788 Estuary, Portugal\), *J. Sea Res.*, 93\(February\), 101–111, doi:10.1016/j.seares.2014.01.003, 2014.](https://doi.org/10.1016/j.seares.2014.01.003)

789 Dutay, J. C., Tagliabue, A., Kriest, I. and van Hulten, M. M. P.: Modelling the role of marine particle on large
790 scale 231Pa, 230Th, Iron and Aluminium distributions, *Prog. Oceanogr.*, 133, 66–72,
791 doi:10.1016/j.poccean.2015.01.010, 2015.

792 [Dutkiewicz, A., Müller, R. D., O'Callaghan, S. and Jónasson, H.: Census of seafloor sediments in the world's
793 ocean, *Geology*, 43\(9\), 795–798, doi:10.1130/G36883.1, 2015.](https://doi.org/10.1130/G36883.1)

794 Eittrheim, S., Thorndike, E. M. and Sullivan, L.: Turbidity distribution in the Atlantic Ocean, *Deep. Res.*
795 *Oceanogr. Abstr.*, 23(12), 1115–1127, doi:10.1016/0011-7471(76)90888-3, 1976.

796 Elderfield, H. and Schultz, A.: Mid-Ocean Ridge Hydrothermal Fluxes and the Chemical Composition of the
797 Ocean, *Annu. Rev. Earth Planet. Sci.*, 24(1), 191–224, doi:10.1146/annurev.earth.24.1.191, 1996.

798 Ellwood, M. J., Nodder, S. D., King, A. L., Hutchins, D. A., Wilhelm, S. W. and Boyd, P. W.: Pelagic iron
799 cycling during the subtropical spring bloom, east of New Zealand, *Mar. Chem.*, 160, 18–33,
800 doi:10.1016/j.marchem.2014.01.004, 2014.

801 Elrod, V. A., Berelson, W. M., Coale, K. H. and Johnson, K. S.: The flux of iron from continental shelf
802 sediments: A missing source for global budgets, *Geophys. Res. Lett.*, 31(12), 2–5, doi:10.1029/2004GL020216,
803 2004.

804 Fitzwater, S. E., Johnson, K. S., Gordon, R. M., Coale, K. H. and Smith, W. O.: Trace metal concentrations in
805 the Ross Sea and their relationship with nutrients and phytoplankton growth, *Deep. Res. Part II Top. Stud.*
806 *Oceanogr.*, 47(15–16), 3159–3179, doi:10.1016/S0967-0645(00)00063-1, 2000.

807 Fragoso, G. M., Poulton, A. J., Yashayaev, I. M., Head, E. J. H., Stinchcombe, M. C. and Purdie, D. A.:
808 Biogeographical patterns and environmental controls of phytoplankton communities from contrasting
809 hydrographical zones of the Labrador Sea, *Prog. Oceanogr.*, 141, 212–226, doi:10.1016/j.pocean.2015.12.007,
810 2016.

811 Frew, R. D., Hutchins, D. A., Nodder, S., Sanudo-Wilhelmy, S., Tovar-Sanchez, A., Leblanc, K., Hare, C. E.
812 and Boyd, P. W.: Particulate iron dynamics during FeCycle in subantarctic waters southeast of New Zealand,
813 *Global Biogeochem. Cycles*, 20(1), 1–15, doi:10.1029/2005GB002558, 2006.

814 García-Ibáñez, M. I., Pardo, P. C., Carracedo, L. I., Mercier, H., Lherminier, P., Ríos, A. F. and Pérez, F. F.:
815 Structure, transports and transformations of the water masses in the Atlantic Subpolar Gyre, *Prog. Oceanogr.*,
816 135, 18–36, doi:10.1016/j.pocean.2015.03.009, 2015.

817 Gardner, W. D., Tucholke, B. E., Richardson, M. J. and Biscaye, P. E.: Benthic storms, nepheloid layers, and
818 linkage with upper ocean dynamics in the western North Atlantic, *Mar. Geol.*, 385, 304–327,
819 doi:10.1016/j.margeo.2016.12.012, 2017.

820 Gardner, W. D., Richardson, M. J. and Mishonov, A. V.: Global assessment of benthic nepheloid layers and
821 linkage with upper ocean dynamics, *Earth Planet. Sci. Lett.*, 482, 126–134, doi:10.1016/j.epsl.2017.11.008,
822 2018.

823 Gerringa, L. J. A., Rijkenberg, M. J. A., Schoemann, V., Laan, P. and de Baar, H. J. W.: Organic complexation
824 of iron in the West Atlantic Ocean, *Mar. Chem.*, 177, 434–446, doi:10.1016/j.marchem.2015.04.007, 2015.

825 Hawkings, J. R., Wadham, J. L., Tranter, M., Raiswell, R., Benning, L. G., Statham, P. J., Tedstone, A.,
826 Nienow, P., Lee, K. and Telling, J.: Ice sheets as a significant source of highly reactive nanoparticulate iron to
827 the oceans, *Nat. Commun.*, 5(May), 1–8, doi:10.1038/ncomms4929, 2014.

828 Hwang, J., Druffel, E. R. M. and Eglinton, T. I.: Widespread influence of resuspended sediments on oceanic
829 particulate organic carbon: Insights from radiocarbon and aluminum contents in sinking particles, *Global*
830 *Biogeochem. Cycles*, 24(4), 1–10, doi:10.1029/2010GB003802, 2010.

831 Jeandel, C. and Oelkers, E. H.: The influence of terrigenous particulate material dissolution on ocean chemistry
832 and global element cycles, *Chem. Geol.*, 395, 50–66, doi:10.1016/j.chemgeo.2014.12.001, 2015.

833 Jeandel, C., Peucker-Ehrenbrink, B., Jones, M. T., Pearce, C. R., Oelkers, E. H., Godderis, Y., Lacan, F.,
834 Aumont, O. and Arsouze, T.: Ocean margins: The missing term in oceanic element budgets?, *Eos, Transactions*
835 *American Geophysical Union*, 92(26), 217–224, doi: 10.1029/2011EO260001, 2011.

836 Jickells, T. D., An, Z. S., Andersen, K. K., Baker, A. R., Bergametti, C., Brooks, N., Cao, J. J., Boyd, P. W.,
837 Duce, R. A., Hunter, K. A., Kawahata, H., Kubilay, N., LaRoche, J., Liss, P. S., Mahowald, N., Prospero, J. M.,
838 Ridgwell, A. J., Tegen, I. and Torres, R.: Global iron connections between desert dust, ocean biogeochemistry,
839 and climate, *Science* (80-.), 308(5718), 67–71, doi:10.1126/science.1105959, 2005.

840 Jouanneau, J. M., Garcia, C., Oliveira, A., Rodrigues, A., Dias, J. A. and Weber, O.: Dispersal and deposition of
841 suspended sediment on the shelf off the Tagus and Sado estuaries, S.W. Portugal, *Prog. Oceanogr.*, 42(1–4),
842 233–257, doi:10.1016/S0079-6611(98)00036-6, 1998.

843 Labatut, M., Lacan, F., Pradoux, C., Chmeleff, J., Radic, A., Murray, J. W., Poitrasson, F., Johansen, A. M.,
844 Thil, F., Lacan, F., Pradoux, C., Chmeleff, J., Radic, A., Murray, J. W., Poitrasson, F., Johansen, A. M. and
845 Thil, F.: Iron sources and dissolved - particulate interactions in the seawater of the Western Equatorial Pacific,
846 iron isotope perspectives., *Global Biogeochem Cycles*~~*Global Biogeochemical Cycles*~~, 1044–1065,
847 doi:10.1002/2014GB004928, 2014.

848 Lam, P. J. and Bishop, J. K. B.: The continental margin is a key source of iron to the HNLC North Pacific
849 Ocean, *Geophys. Res. Lett.*, 35(7), 1–5, doi:10.1029/2008GL033294, 2008.

850 Lam, P. J., Ohnemus, D. C. and Marcus, M. A.: The speciation of marine particulate iron adjacent to active and
851 passive continental margins, *Geochim. Cosmochim. Acta*, 80, 108–124, doi:10.1016/j.gca.2011.11.044, 2012.

852 Lam, P. J., Ohnemus, D. C. and Auro, M. E.: Size-fractionated major particle composition and concentrations
853 from the US GEOTRACES North Atlantic Zonal Transect, *Deep. Res. Part II Top. Stud. Oceanogr.*, 116, 303–
854 320, doi:10.1016/j.dsr2.2014.11.020, 2015.

855 Lam, P. J., Lee, J. M., Heller, M. I., Mehic, S., Xiang, Y. and Bates, N. R.: Size-fractionated distributions of
856 suspended particle concentration and major phase composition from the U.S. GEOTRACES Eastern Pacific
857 Zonal Transect (GP16), *Mar. Chem.*, (April), 0–1, doi:10.1016/j.marchem.2017.08.013, 2017.

858 Lannuzel, D., Bowie, A. R., van der Merwe, P. C., Townsend, A. T. and Schoemann, V.: Distribution of
859 dissolved and particulate metals in Antarctic sea ice, *Mar. Chem.*, 124(1–4), 134–146,
860 doi:10.1016/j.marchem.2011.01.004, 2011.

861 Lannuzel, D., Van der Merwe, P. C., Townsend, A. T. and Bowie, A. R.: Size fractionation of iron, manganese
862 and aluminium in Antarctic fast ice reveals a lithogenic origin and low iron solubility, *Mar. Chem.*, 161, 47–56,
863 doi:10.1016/j.marchem.2014.02.006, 2014.

864 Lee, J. M., Heller, M. I. and Lam, P. J.: Size distribution of particulate trace elements in the U.S. GEOTRACES
865 Eastern Pacific Zonal Transect (GP16), *Mar. Chem.*, 201(September 2017), 108–123,
866 doi:10.1016/j.marchem.2017.09.006, 2017.

867 Lemaitre, N., Planquette, H., Planchon, F., Sarthou, G., Jacquet, S., Garcia-Ibanez, M. I., Gourain, A., Cheize,
868 M., Monin, L., Andre, L., Laha, P., Terryn, H., and Dehairs, F.: Particulate barium tracing significant
869 mesopelagic carbon remineralisation in the North Atlantic, *Biogeosciences–Discussions*, doi:10.5194/bg-15-
870 2289-2018, 2018a.

871 Lemaitre, N., Planchon, F., Planquette, H., Dehairs, F., Fonseca-Batista, D., Roukaerts, A., Deman, F., Tang, Y.,
872 Mariez, C., and Sarthou G.: High variability of export fluxes along the North Atlantic GEOTRACES section
873 GA01: Particulate organic carbon export deduced from the 234Th method, *Biogeosciences–Discuss.*,
874 doi:10.5194/bg-2018-190, 2018b.

875 Le Roy, E., Sanial, V., Charette, M.A., Van Beek, P., Lacan, F., Jacquet, S.H., Henderson, P.B., Souhaut, M.,
876 García-Ibáñez, M.I., Jeandel, C. and Pérez, F.: The 226Ra-Ba relationship in the North Atlantic during
877 GEOTRACES-GA01, *Biogeosciences–Discussions*, doi:10.5194/bg-2017-478, 2017.

878 ~~Loring, D. H. and Asmund, G.: Geochemical factors controlling accumulation of major and trace elements in
879 Greenland coastal and fjord sediments, *Environ. Geol.*, 28(1), 2–11, doi:10.1007/s002540050072, 1996.~~

880 ~~Mahowald, N. M., Baker, A. R., Bergametti, G., Brooks, N., Duce, R. A., Jickells, T. D., Kubilay, N., Prospero,
881 J. M. and Tegen, I.: Atmospheric global dust cycle and iron inputs to the ocean, *Global Biogeochem. Cycles*,
882 19(4), doi:10.1029/2004GB002402, 2005.~~

883 Marsay, C. M., Lam, P. J., Heller, M. I., Lee, J. M. and John, S. G.: Distribution and isotopic signature of
884 ligand-leachable particulate iron along the GEOTRACES GP16 East Pacific Zonal Transect, *Mar. Chem.*,
885 (November 2016), 1–14, doi:10.1016/j.marchem.2017.07.003, 2017.

886 Martin, J. H., Fitzwater, S. E., Michael Gordon, R., Hunter, C. N. and Tanner, S. J.: Iron, primary production
887 and carbon-nitrogen flux studies during the JGOFS North Atlantic bloom experiment, *Deep. Res. Part II*, 40(1–
888 2), 115–134, doi:10.1016/0967-0645(93)90009-C, 1993.

889 McCave, I. N. and Hall, I. R.: Turbidity of waters over the Northwest Iberian continental margin, *Prog.*
890 *Oceanogr.*, 52(2–4), 299–313, doi:10.1016/S0079-6611(02)00012-5, 2002.

891 Menzel Barraqueta, J.L., Schlosser, C., Planquette, H., Gourain, A., Cheize, M., Boutorh, J., Shelley, R., Pereira
892 Contreira, L., Gledhill, M., Hopwood, M.J. and Lherminier, P.: Aluminium in the North Atlantic Ocean and the
893 Labrador Sea (GEOTRACES GA01 section): roles of continental inputs and biogenic particle removal.
894 *Biogeosciences–Discussions*, 1-28, doi: 10.5194/bg-2018-39, 2018.

895 Milne, A., Schlosser, C., Wake, B. D., Achterberg, E. P., Chance, R., Baker, A. R., Forryan, A. and Lohan, M.
896 C.: Particulate phases are key in controlling dissolved iron concentrations in the (sub)tropical North Atlantic,
897 *Geophys. Res. Lett.*, 44(5), 2377–2387, doi:10.1002/2016GL072314, 2017.

898 ~~Mudie, P. J., Keen, C. E., Hardy, I. A. and Vilks, G.: Multivariate analysis and quantitative paleoecology of~~
899 ~~benthic foraminifera in surface and Late Quaternary shelf sediments, northern Canada, *Mar. Micropaleontol.*,~~
900 ~~8(4), 283–313, doi:10.1016/0377-8398(84)90018-5, 1984.~~

901 Nuester, J., Shema, S., Vermont, A., Fields, D. M. and Twining, B. S.: The regeneration of highly bioavailable
902 iron by meso- and microzooplankton, *Limnol. Oceanogr.*, 59(4), 1399–1409, doi:10.4319/lo.2014.59.4.1399,
903 2014.

904 Oelkers, E. H., Jones, M. T., Pearce, C. R., Jeandel, C., Eiriksdottir, E. S. and Gislason, S. R.: Riverine
905 particulate material dissolution in seawater and its implications for the global cycles of the elements, *Geosci.*,
906 344(11–12), 646–651, doi:10.1016/j.crte.2012.08.005, 2012.

907 Ohnemus, D. C. and Lam, P. J.: Cycling of lithogenic marine particles in the US GEOTRACES North Atlantic
908 transect, *Deep. Res. Part II Top. Stud. Oceanogr.*, 116, 283–302, doi:10.1016/j.dsr2.2014.11.019, 2015.

909 Peers, G. and Price, N. M.: A role for manganese in superoxide dismutases and growth of iron-deficient
910 diatoms, *Limnol. Oceanogr.*, 49(5), 1774–1783, doi:10.4319/lo.2004.49.5.1774, 2004.

911 Planquette, H. and Sherrell, R. M.: Sampling for particulate trace element determination using water sampling
912 bottles: Methodology and comparison to in situ pumps, *Limnol. Oceanogr. Methods*, 10(5), 367–388,
913 doi:10.4319/lom.2012.10.367, 2012.

914 Planquette, H., Fones, G. R., Statham, P. J. and Morris, P. J.: Origin of iron and aluminium in large particles (>
915 53 μm) in the Crozet region, Southern Ocean, *Mar. Chem.*, 115(1–2), 31–42,
916 doi:10.1016/j.marchem.2009.06.002, 2009.

917 Planquette, H., Sanders, R. R., Statham, P. J., Morris, P. J. and Fones, G. R.: Fluxes of particulate iron from the
918 upper ocean around the Crozet Islands: A naturally iron-fertilized environment in the Southern Ocean, *Global*
919 *Biogeochem. Cycles*, 25(2), doi:10.1029/2010GB003789, 2011.

920 Planquette, H., Sherrell, R. M., Stammerjohn, S. and Field, M. P.: Particulate iron delivery to the water column
921 of the Amundsen Sea, Antarctica, *Mar. Chem.*, 153, 15–30, doi:10.1016/j.marchem.2013.04.006, 2013.

922 Radic, A., Lacan, F. and Murray, J. W.: Iron isotopes in the seawater of the equatorial Pacific Ocean: New
923 constraints for the oceanic iron cycle, *Earth Planet. Sci. Lett.*, 306(1–2), 1–10, doi:10.1016/j.epsl.2011.03.015,
924 2011.

925 Raiswell, R., Benning, L. G., Tranter, M. and Tulaczyk, S.: Bioavailable iron in the Southern Ocean: The
926 significance of the iceberg conveyor belt, *Geochem. Trans.*, 9(1), 7, doi:10.1186/1467-4866-9-7, 2008.

Formatted: English (United Kingdom)

927 Rijkenberg, M. J. A., Middag, R., Laan, P., Gerringa, L. J. A., Van Aken, H. M., Schoemann, V., De Jong, J. T.
928 M. and De Baar, H. J. W.: The distribution of dissolved iron in the West Atlantic Ocean, PLoS One, 9(6), 1–14,
929 doi:10.1371/journal.pone.0101323, 2014.

930 [Rutgers Van Der Loeff, M. M., Meyer, R., Rudels, B. and Rachor, E.: Resuspension and particle transport in the](#)
931 [benthic nepheloid layer in and near Fram Strait in relation to faunal abundances and ²³⁴Th depletion, Deep-](#)
932 [Res. Part I Oceanogr. Res. Pap., 49\(11\), 1941–1958, doi:10.1016/S0967-0637\(02\)00113-9, 2002.](#)

933 Sanders, R., Henson, S. A., Koski, M., De La Rocha, C. L., Painter, S. C., Poulton, A. J., Riley, J., Salihoglu, B.,
934 Visser, A., Yool, A., Bellerby, R. and Martin, A. P.: The Biological Carbon Pump in the North Atlantic, Prog.
935 Oceanogr., 129(PB), 200–218, doi:10.1016/j.pocean.2014.05.005, 2014.

936 [Sarthou, G., Lherminier, and the GEOVIDE team: Introduction to the French GEOTRACES North Atlantic](#)
937 [Transect \(GA01\): GEOVIDE cruise, Biogeosciences, 15, 7097-7109, <https://doi.org/10.5194/bg-15-7097-2018>,](#)
938 [2018.](#)

939

940 Sarthou, G., Vincent, D., Christaki, U., Obernosterer, I., Timmermans, K. R. and Brussaard, C. P. D.: The fate
941 of biogenic iron during a phytoplankton bloom induced by natural fertilisation: Impact of copepod grazing,
942 Deep. Res. Part II Top. Stud. Oceanogr., 55(5–7), 734–751, doi:10.1016/j.dsr2.2007.12.033, 2008.

943 Schlosser, C., Schmidt, K., Aquilina, A., Homoky, W. B., Castrillejo, M., Mills, R. A., Patey, M. D., Fielding,
944 S., Atkinson, A. and Achterberg, E. P.: Mechanisms of dissolved and labile particulate iron supply to shelf
945 waters and phytoplankton blooms off South Georgia, Southern Ocean, Biogeosciences Discuss., 0049(July), 1–
946 49, doi:10.5194/bg-2017-299, 2017.

947 Shelley, R. U., Landing, W. M., Ussher, S. J., Planquett, H. and Sarthou, G.: Characterisation of aerosol
948 provenance from the fractional solubility of Fe (Al, Ti, Mn, Co, Ni, Cu, Zn, Cd and Pb) in North Atlantic
949 aerosols (GEOTRACES GA01 and GA03), Biogeosciences, submitted(November), 1–31, doi:10.5194/bg-
950 2017-415, 2017.

951 Shelley, R. U., Landing, W. M., Ussher, S. J., Planquette, H. and Sarthou, G.: Regional trends in the fractional
952 solubility of Fe and other metals from North Atlantic aerosols (GEOTRACES cruises GA01 and GA03)
953 following a two-stage leach, Biogeosciences, 15(1), 2271–2288, doi:10.5194/bg-15-2271-2018, 2018.

954 Sherrell, R. M., Field, P. M. and Gao, Y.: Temporal variability of suspended mass and composition in the
955 Northeast Pacific water column: Relationships to sinking flux and lateral advection, Deep. Res. Part II Top.
956 Stud. Oceanogr., 45(4–5), 733–761, doi:10.1016/S0967-0645(97)00100-8, 1998.

957 Spinrad, R. W., Zaneveld, J. R. and Kitchen, J.C.: A Study of the Optical Characteristics of the Suspended
958 Particles Benthic Nepheloid Layer of the Scotian Rise, J. Geophys. Res., 88, 7641–7645, doi:10.1029/
959 10.1029/JD083i03C, 1983.

960 Statham, P. J., Skidmore, M. and Tranter, M.: Inputs of glacially derived dissolved and colloidal iron to the
961 coastal ocean and implications for primary productivity, *Global Biogeochem. Cycles*, 22(3), 1–11,
962 doi:10.1029/2007GB003106, 2008.

963 Straneo, F., Pickart, R. S. and Lavender, K.: Spreading of Labrador sea water: An advective-diffusive study
964 based on Lagrangian data, *Deep. Res. Part I Oceanogr. Res. Pap.*, 50(6), 701–719, doi:10.1016/S0967-
965 0637(03)00057-8, 2003.

966 Sunda, W. G. and Huntsman, S. A.: Effect of Competitive Interactions Between Manganese and Copper on
967 Cellular Manganese and Growth in Estuarine and Oceanic Species of the Diatom *Thalassiosira*, *Limnol.*
968 *Oceanogr.*, 28(5), 924–934, doi:10.4319/lo.1983.28.5.0924, 1983.

969 Tagliabue, A., Bopp, L., Dutay, J. C., Bowie, A. R., Chever, F., Jean-Baptiste, P., Bucciarelli, E., Lannuzel, D.,
970 Remenyi, T., Sarthou, G., Aumont, O., Gehlen, M. and Jeandel, C.: Hydrothermal contribution to the oceanic
971 dissolved iron inventory, *Nat. Geosci.*, 3(4), 252–256, doi:10.1038/ngeo818, 2010.

972 Tagliabue, A., Bowie, A. R., Boyd, P. W., Buck, K. N., Johnson, K. S. and Saito, M. A.: The integral role of
973 iron in ocean biogeochemistry, *Nature*, 543(7643), 51–59, doi:10.1038/nature21058, 2017.

974 Taylor, S. and McLennan, S.: The geochemical evolution of the continental crust, *Rev. Geophys.*, 33(2), 241–
975 265, doi:10.1029/95RG00262, 1995.

976 Tebo, B. M. and Emerson, S. R.: Effect of Oxygen Tension Manganese (II) Concentration and Temperature on
977 the Microbially Catalyzed Manganese-Iron Oxidation Rate in a Marine Fjord, *Appl. Environ. Microbiol.*, 50(5),
978 1268–1273, 1985.

979 Tebo, B. M., Neelson, K. H., Emerson, S. and Jacobs, L.: Microbial mediation of Mn(II) and Co(II)
980 precipitation at the $\text{O}_2/\text{H}_2\text{S}$ interfaces in two anoxic fjords, 29(6), 1247–1258, 1984.

981 Tonnard, M., Planquette, H., Bowie, A. R., van der Merwe, P., Gallinari, M., Desprez de Gésincourt, F.,
982 Germain, Y., Gourain, A., Benetti, M., Reverdin, G., Tréguer, P., Boutorh, J., Cheize, M., Menzel Barraqueta,
983 J., Pereira-Contreira, L., Shelley, R., Lherminier, P., and Sarthou, G.: Dissolved iron in the North Atlantic
984 Ocean and Labrador Sea along the GEOVIDE section (GEOTRACES section GA01), *Biogeosciences Discuss.*,
985 <https://doi.org/10.5194/bg-2018-147>, 2018

986 Trefry, J. H., Trocine, R. P., Klinkhammer, G. P. and Rona, P. A.: Iron and copper enrichment of suspended
987 particles in dispersed hydrothermal plumes along the mid-Atlantic Ridge, *Geophys. Res. Lett.*, 12(8), 506–
988 509, doi:10.1029/GL012i008p00506, 1985.

989 Ussher, S. J., Achterberg, E. P. and Worsfold, P. J.: Marine biogeochemistry of iron, *Environ. Chem.*, 1(2), 67–
990 80, doi:10.1071/EN04053, 2004.

991 Ussher, S. J., Worsfold, P. J., Achterberg, E. P., Laës, A., Blain, S., Laan, P., de Baar, H. J. W.: Distribution and
992 redox speciation of dissolved iron on the European continental margin, *Limnol. Oceanogr.*, 52(6), 2530–2539,
993 doi:10.4319/lo.2007.52.6.2530, 2007.

994 Van der Merwe, P., Lannuzel, D., Bowie, A. R., Mancuso Nichols, C. A. and Meiners, K. M.: Iron fractionation
995 in pack and fast ice in East Antarctica: Temporal decoupling between the release of dissolved and particulate
996 iron during spring melt, *Deep. Res. Part II Top. Stud. Oceanogr.*, 58(9–10), 1222–1236,
997 doi:10.1016/j.dsr2.2010.10.036, 2011a.

998 Van Der Merwe, P., Lannuzel, D., Bowie, A. R. and Meiners, K. M.: High temporal resolution observations of
999 spring fast ice melt and seawater iron enrichment in East Antarctica, *J. Geophys. Res. Biogeosciences*, 116(3),
1000 1–18, doi:10.1029/2010JG001628, 2011b.

1001 Weinstein, S. E. and Moran, S. B.: Distribution of size-fractionated particulate trace metals collected by bottles
1002 and in-situ pumps in the Gulf of Maine-Scotian Shelf and Labrador Sea, *Mar. Chem.*, 87(3–4), 121–135,
1003 doi:10.1016/j.marchem.2004.02.004, 2004.

1004 Yashayaev, I.: Hydrographic changes in the Labrador Sea, 1960-2005, *Prog. Oceanogr.*, 73(3–4), 242–276,
1005 doi:10.1016/j.pocean.2007.04.015, 2007.

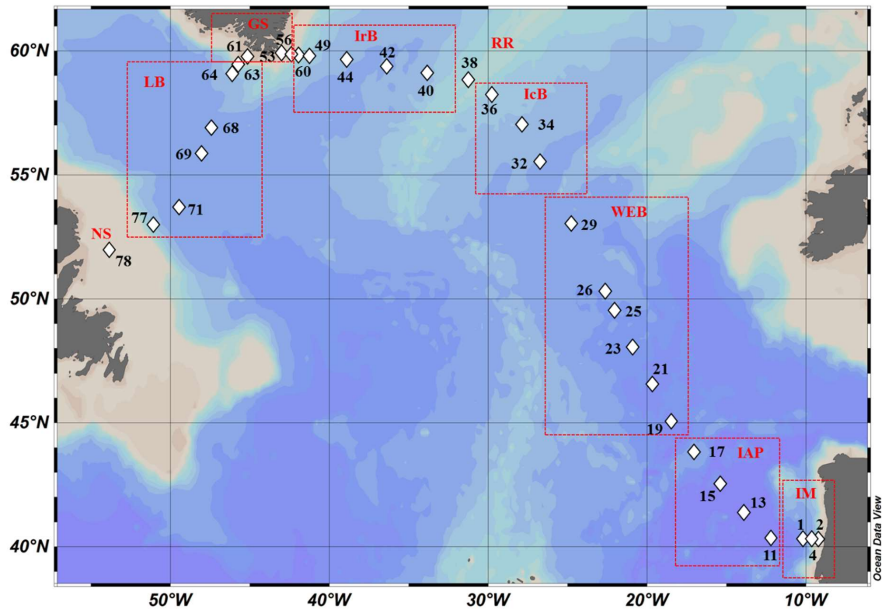
1006 Yashayaev, I. and Loder, J. W.: Enhanced production of Labrador Sea Water in 2008, *Geophys. Res. Lett.*,
1007 36(1), doi:10.1029/2008GL036162, 2009.

1008 Zunino, P., Lherminier, P., Mercier, H., Daniault, N., Garcia-Ibáñez, M. I., and Pérez, F. F.: The GEOVIDE
1009 cruise in May–June 2014 reveals an intense Meridional Overturning Circulation over a cold and fresh subpolar
1010 North Atlantic. *Biogeosciences*, 14(23), 5323, 2017.

1011
1012
1013
1014
1015
1016
1017
1018
1019
1020
1021
1022
1023
1024
1025
1026

1027
1028
1029
1030
1031
1032
1033
1034
1035
1036
1037
1038
1039
1040
1041
1042
1043
1044
1045
1046
1047
1048
1049
1050
1051
1052
1053
1054
1055
1056
1057
1058
1059
1060

1061 **Figure 1: Map of stations where suspended particle samples were collected with GO-FLO bottles during the**
1062 **GEOVIDE cruise (GA01). Biogeochemical provinces are indicated by red squares, IM: Iberian Margin, IAP: Iberian**
1063 **Abyssal Plain, WEB: Western European Basin, IcB: Iceland Basin, RR: Reykjanes Ridge, IrB: Irminger Basin, GS:**
1064 **Greenland Shelf, LB: Labrador Basin, NS: Newfoundland Shelf. This figure was generated by Ocean Data View**
1065 **(Schlitzer, R., Ocean Data View, odv.awi.de, 2017).**



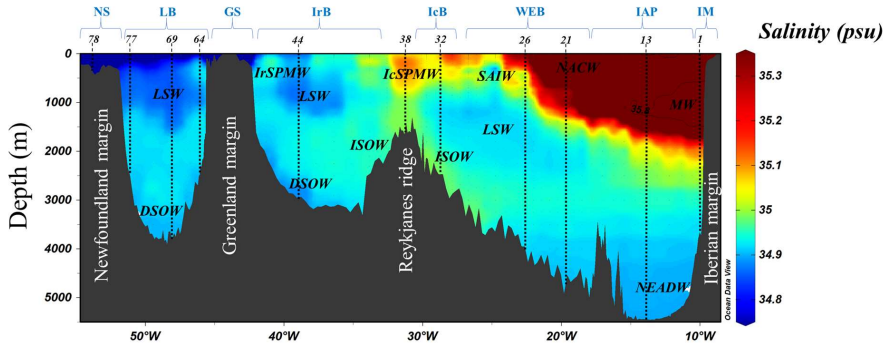
1066
 1067
 1068
 1069
 1070
 1071
 1072
 1073
 1074
 1075
 1076
 1077
 1078
 1079
 1080
 1081

1082 Figure 2: Salinity section during the GEOVIDE cruise. Water masses are indicated in black, MW: Mediterranean
 1083 Water; NACW: North Atlantic Central Water; NEADW: North East Atlantic Deep Water; LSW: Labrador Sea
 1084 Water; **DSOW: Denmark Strait Overflow Water**; ISOW: Iceland-Scotland Overflow Water; SAIW: Sub-Arctic
 1085 Intermediate Water; IcSPMW: Iceland Sub-Polar Mode Water; IrSPMW: Irminger Sub-Polar Mode Water.
 1086 Station locations are indicated by the numbers. Biogeochemical provinces are indicated in blue font above station

1087 numbers. Contour of salinity = 35.8psu have been applied to identify the Mediterranean Water. This figure was
 1088 generated by Ocean Data View (Schlitzer, R., Ocean Data View, odv.awi.de, 2017).

1089

1090



1091

1092

1093

1094

1095

1096

1097

1098

1099

1100

1101

1102

1103

1104

1105

1106

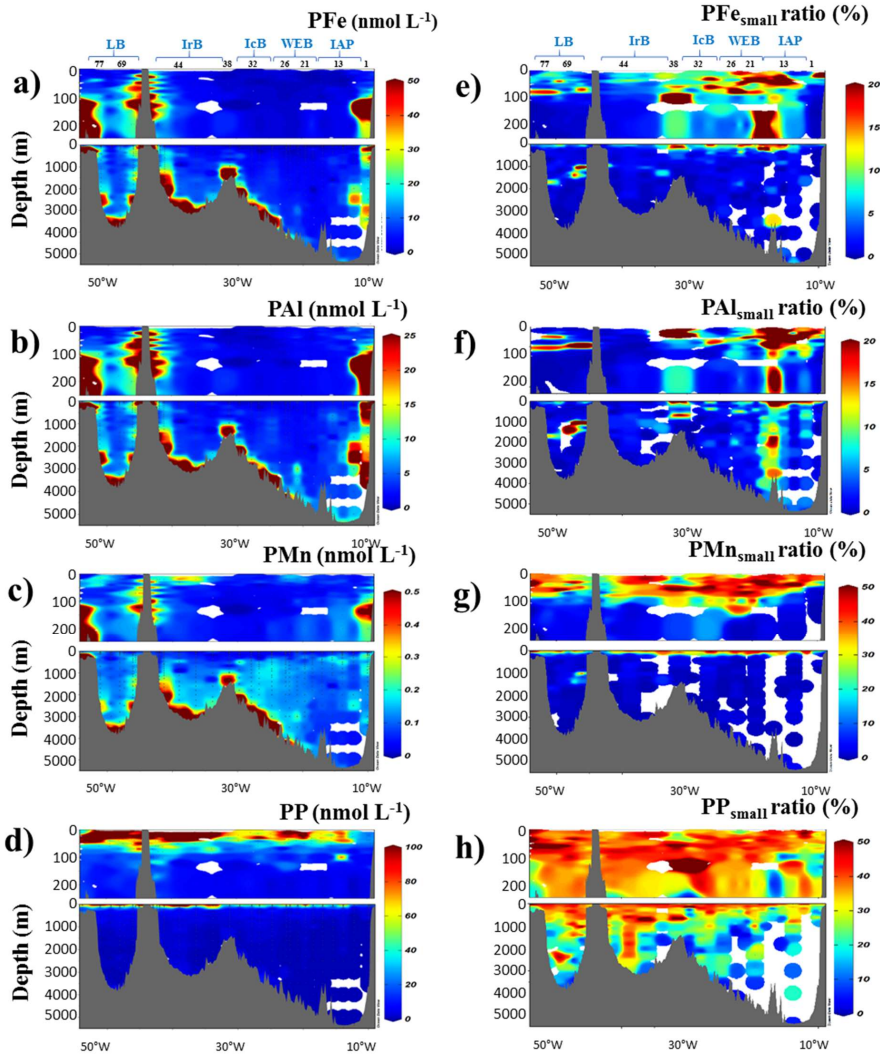
1107

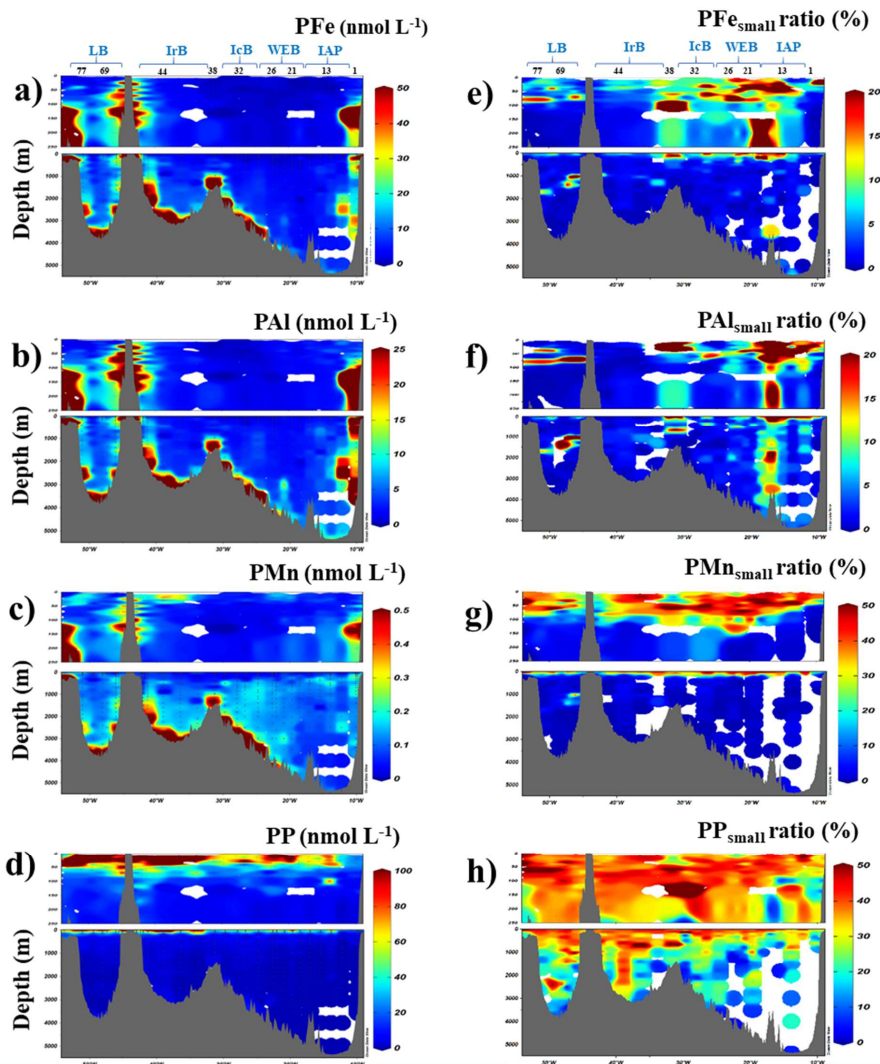
1108

1109

1110

1111 Figure 3: Left) Distribution of total particulate iron (a, PFe), aluminium (b, PAI), manganese (c, PMn) and
 1112 phosphorus (d, PP) concentrations (in nmol L⁻¹) along the GEOVIDE section. Right) Contribution of small size
 1113 fraction (0,45-5 µm) expressed as percentage (%) of the total concentration of PFe (e), PAI (f), PMn (g) and PP (h).
 1114 Station IDs and biogeochemical region are indicated on top of section a. This figure was generated by Ocean Data
 1115 View (Schlitzer, R., Ocean Data View, odv.awi.de, 2017).



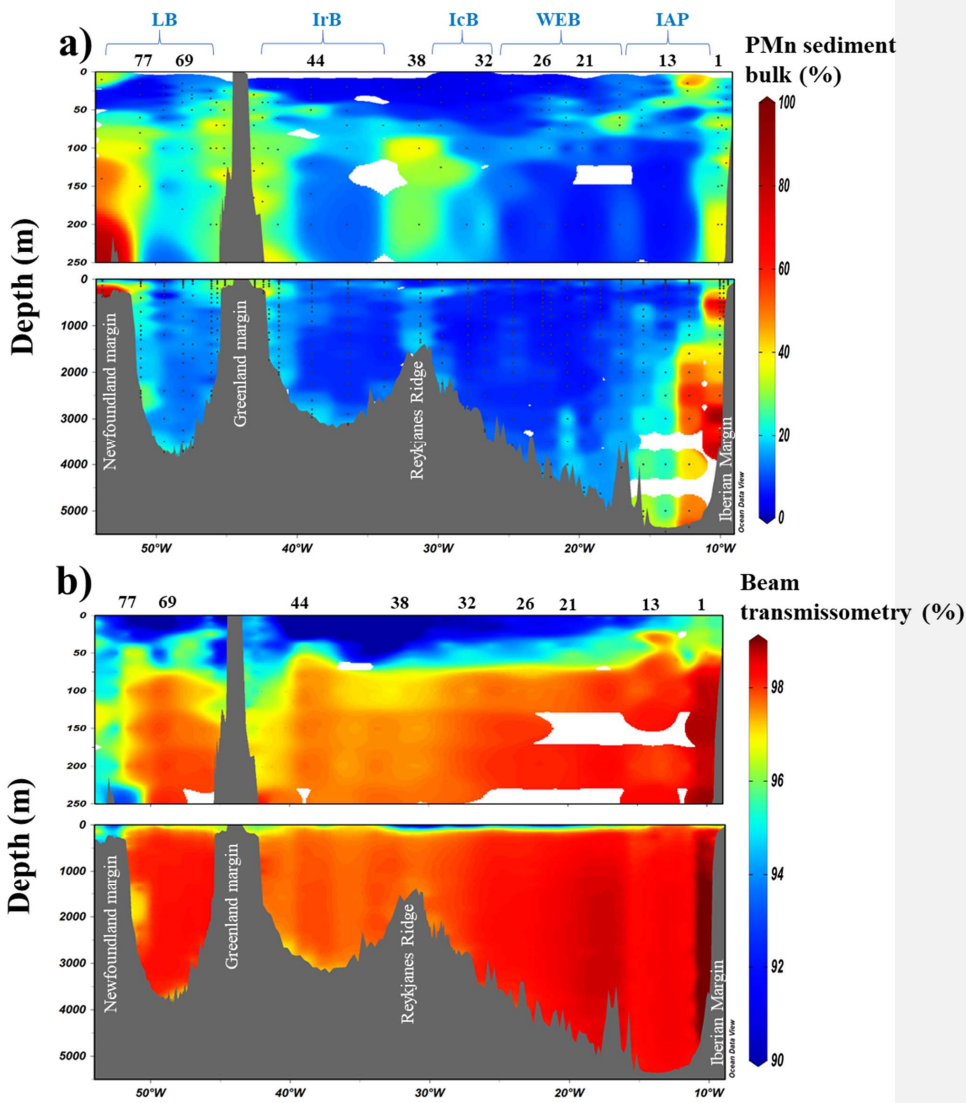


1117

1118

1119

1120 Figure 4: Section of derived contribution of sedimentary inputs manganese bulk sediment proxy (a) and
 1121 transmissometry (b) along the GA01 section. Station IDs and biogeochemical region are indicated above the section
 1122 (a). This figure was generated by Ocean Data View (Schlitzer, R., Ocean Data View, odv.awi.de, 2017).

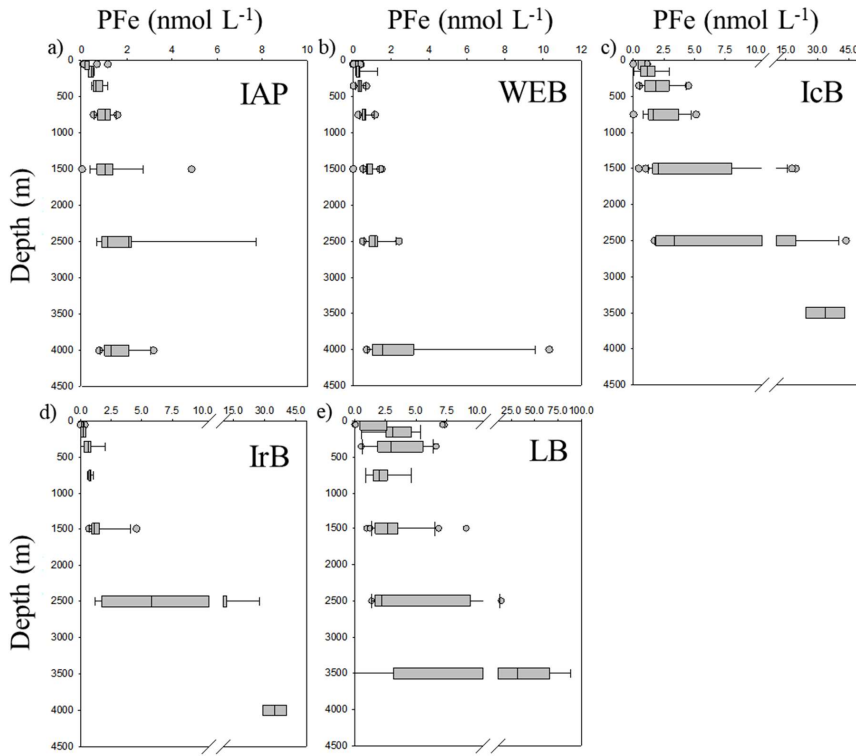


1123
1124
1125
1126

1127 **Figure 4: Boxplot figure of the particulate iron-vertical profile (in nmol L^{-1}) in the a) Iberian abyssal plain (IAP), b)**
 1128 **Western European basin (WEB), c) Icelandic basin (IcB), d) Irminger basin (IrB) and e) Labrador basins (LB).**
 1129 **Please note the change of PFC scale between the basins. The left boundary of the box represents the 25th percentile**
 1130 **while the right boundary represents the 75th percentile, the line within the box marks the median value. Whiskers**

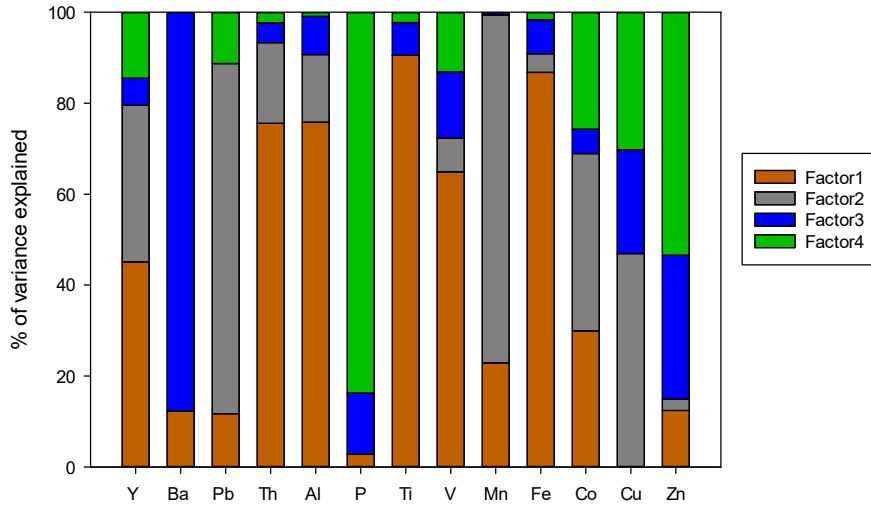
1131
1132

represent the 90th and 10th percentiles and dots are the outlying data. Seven depth boxes have been used (0-100m, 100-200m, 200-500m, 500-1000m, 1000-2000m, 2000-3000m and 3000m-bottom depth).



1133
1134
1135
1136
1137
1138
1139
1140
1141
1142

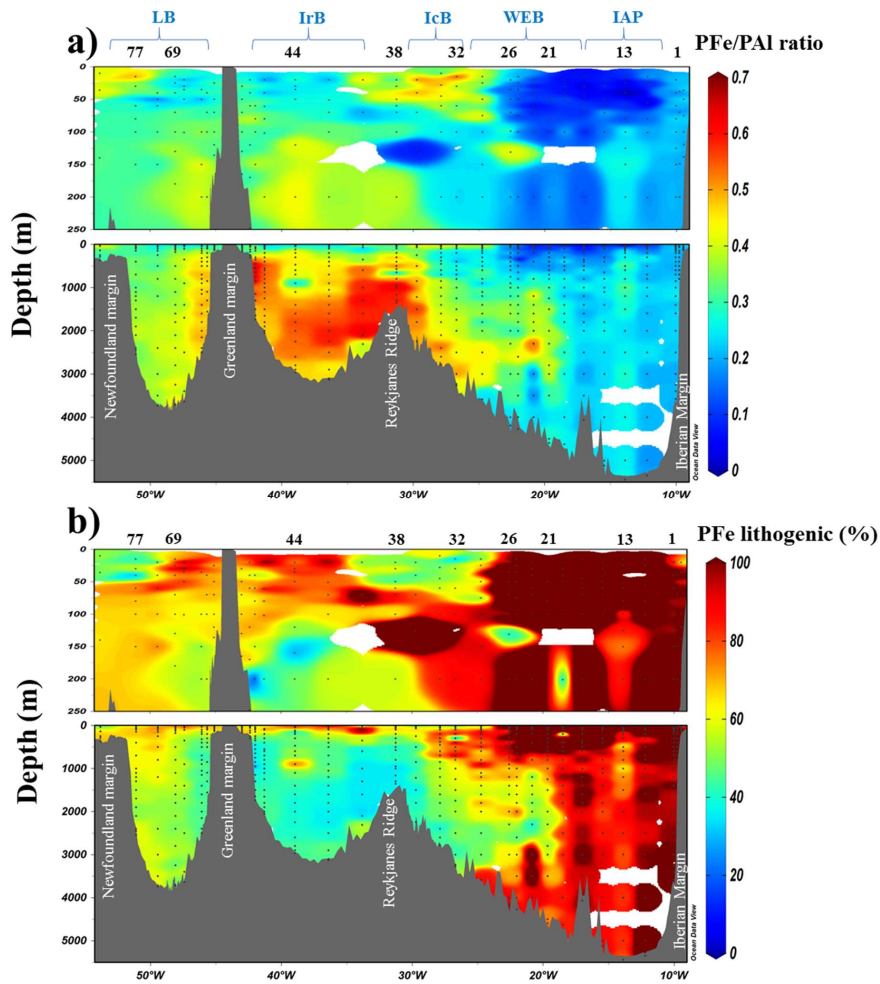
1143 Figure 5: Factor fingerprint of the positive matrix factorisation. The four factors are represented in a stacked bar
1144 chart of the percentage of variance explained per element.



1145
 1146
 1147
 1148
 1149
 1150
 1151
 1152
 1153
 1154
 1155
 1156
 1157
 1158
 1159
 1160
 1161
 1162
 1163

1164 Figure 6: a) Section of the PFe to PAI molar ratio (mol mol^{-1}); (b) contribution of lithogenic $\text{PFe}_{\text{litho}}(\%)$ based on Eq.
 1165 (1). Station IDs and biogeochemical provinces are indicated above each section. This figure was generated by Ocean
 1166 Data View (Schlitzer, R., Ocean Data View, odv.awi.de, 2017).

Formatted: Subscript

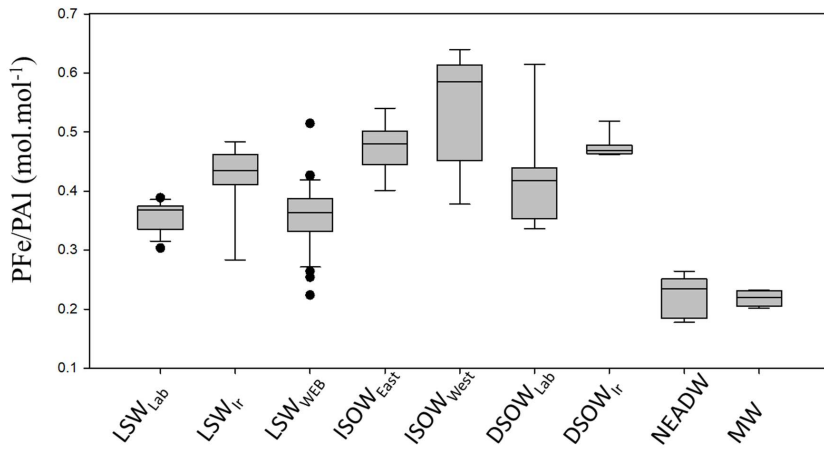


1167
 1168
 1169
 1170
 1171
 1172
 1173
 1174
 1175
 1176
 1177

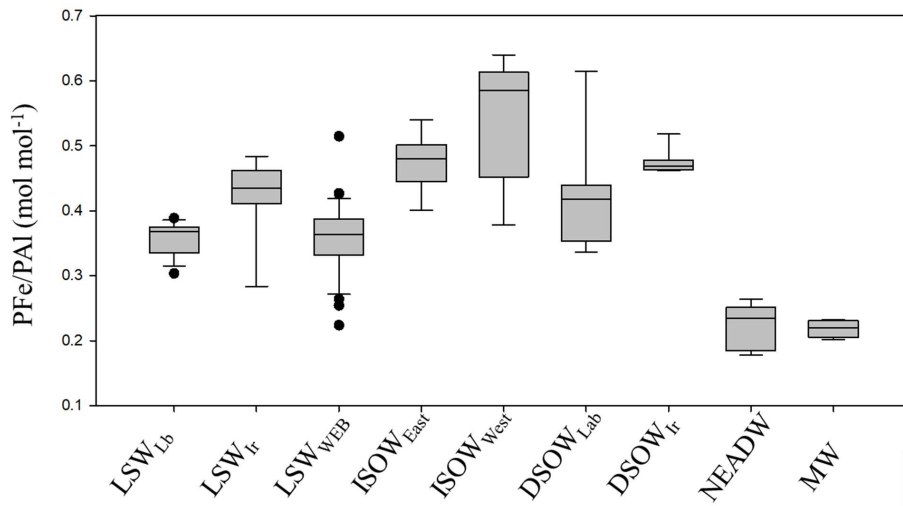
Figure 7: Whisker diagram of PFe/PAI molar ratio (mol mol^{-1}) in the different water masses sampled along the GA01 line. Median values for the water masses were as follows: $\text{LSW}_{\text{lb}}=0.37$; $\text{LSW}_{\text{Ir}}=0.44$; $\text{LSW}_{\text{WEB}}=0.36$; $\text{ISOW}_{\text{east}}=0.48$; $\text{ISOW}_{\text{west}}=0.58$; $\text{DSOW}_{\text{lb}}=0.42$; $\text{DSOW}_{\text{Ir}}=0.47$; $\text{NEADW}=0.23$; $\text{MW}=0.22 \text{ mol mol}^{-1}$. [Based on their salinity and potential temperature signatures \(García-Ibáñez et al., 2015; Figure 2\), we applied a Kruskal-Wallis test on molar](#)

1178
1179
1180
1181

[PFe/PAI ratios of nine water masses \(Figure 7\) in order to test the presence of significant differences. Water masses for which we had less than 5 data points for PFe/PAI were excluded from this test. As the differences in the median values among the treatment groups were greater than would be expected by chance; the difference in PFe/PAI between water masses is statistically significant \(\$P = <0.001\$ \).](#)



1182
1183

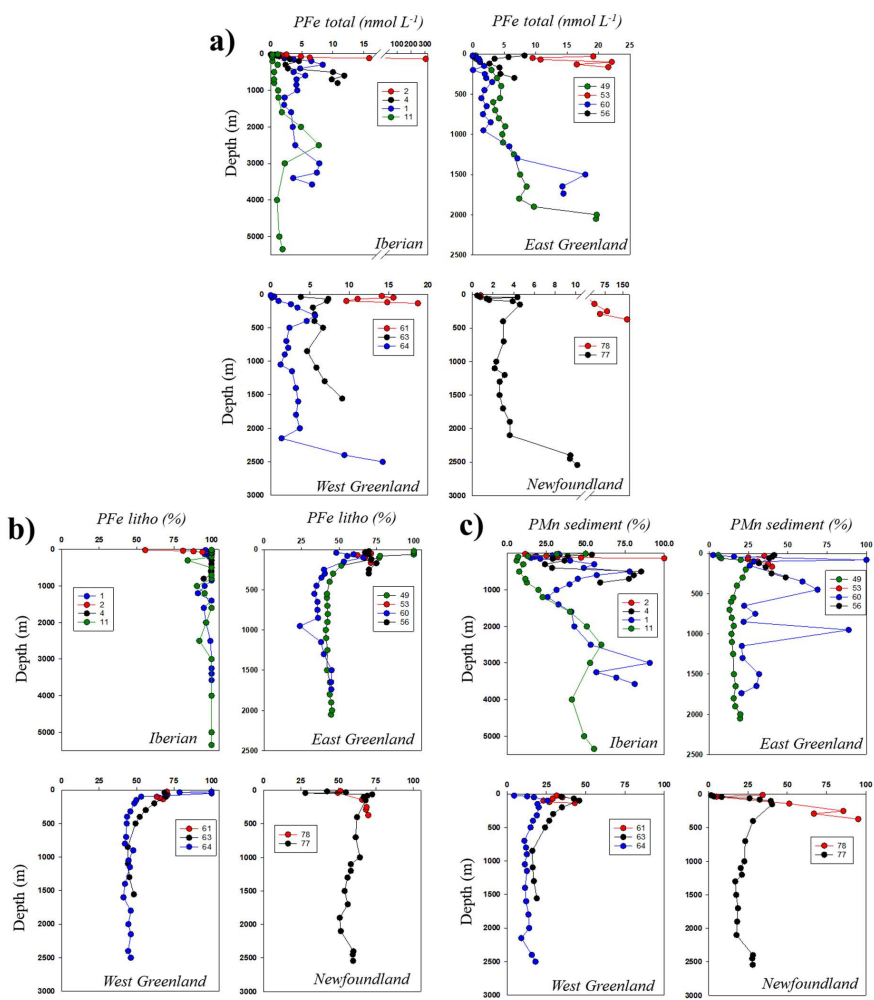


1184
1185
1186
1187

1188
1189
1190
1191
1192
1193
1194
1195
1196
1197

1198 Figure 8: Vertical profiles of PFe (nmol L⁻¹, a), lithogenic proportion of particulate iron (PFe_{litho}, %, b) and
1199 sedimentary proportion of particulate manganese (PMn sediment, %, c) at the Iberian, East-West Greenland and
1200 Newfoundland margins.

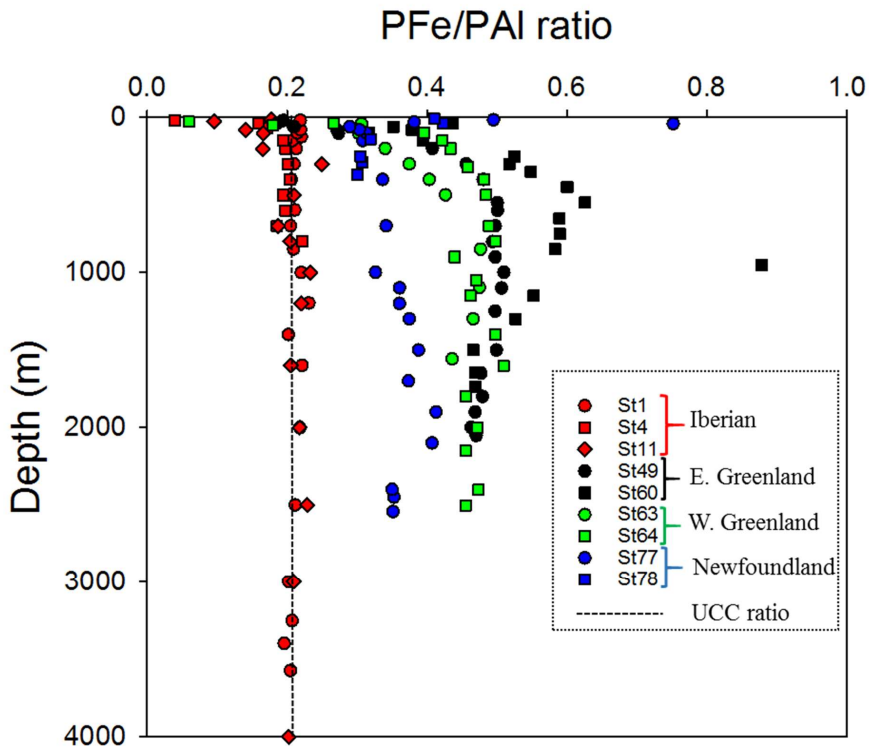
Formatted: Subscript



1201
1202
1203
1204
1205
1206
1207
1208
1209

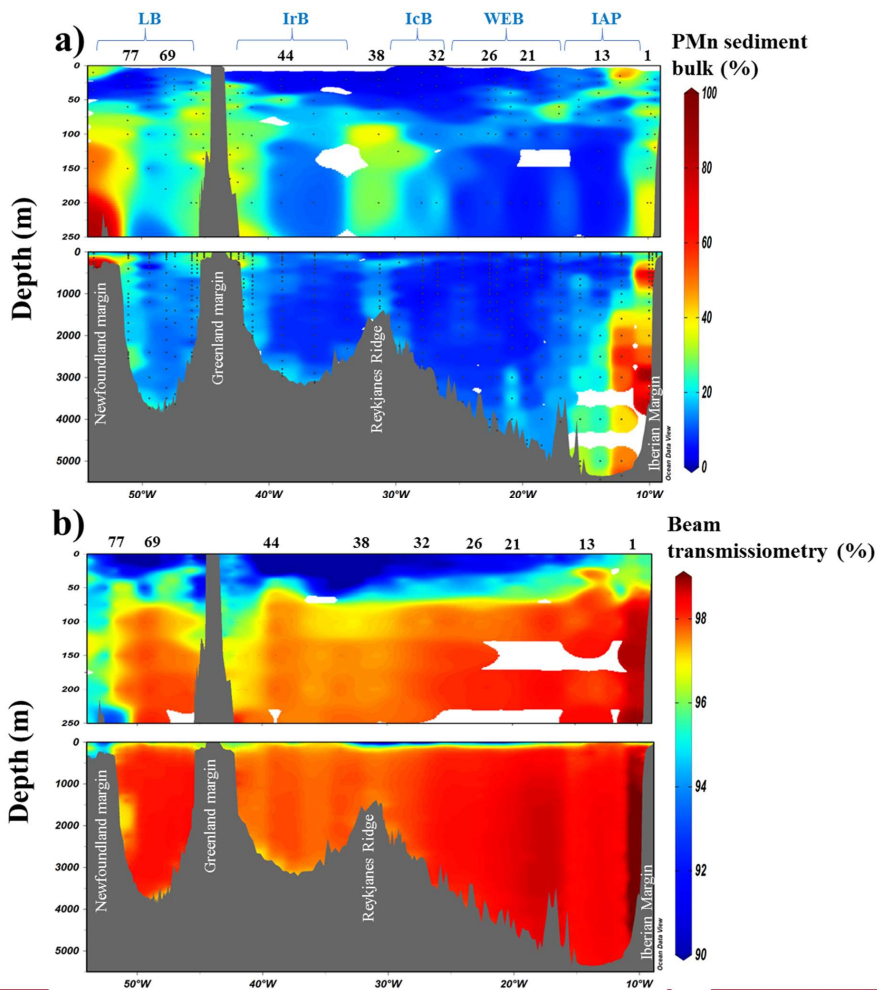
Formatted: Font: (Default) +Body (Calibri), 11 pt
Formatted: Normal, Left

1210 Figure 89: Scatter of the PFe/PAI ratio at the Iberian (red dots), East Greenland (black dots), West Greenland (green
 1211 dots) and Newfoundland margins (blue dots). Dashed line indicate the UCC ratio (Taylor and McLennan, 1995).



1212
 1213
 1214
 1215
 1216
 1217
 1218
 1219
 1220
 1221
 1222

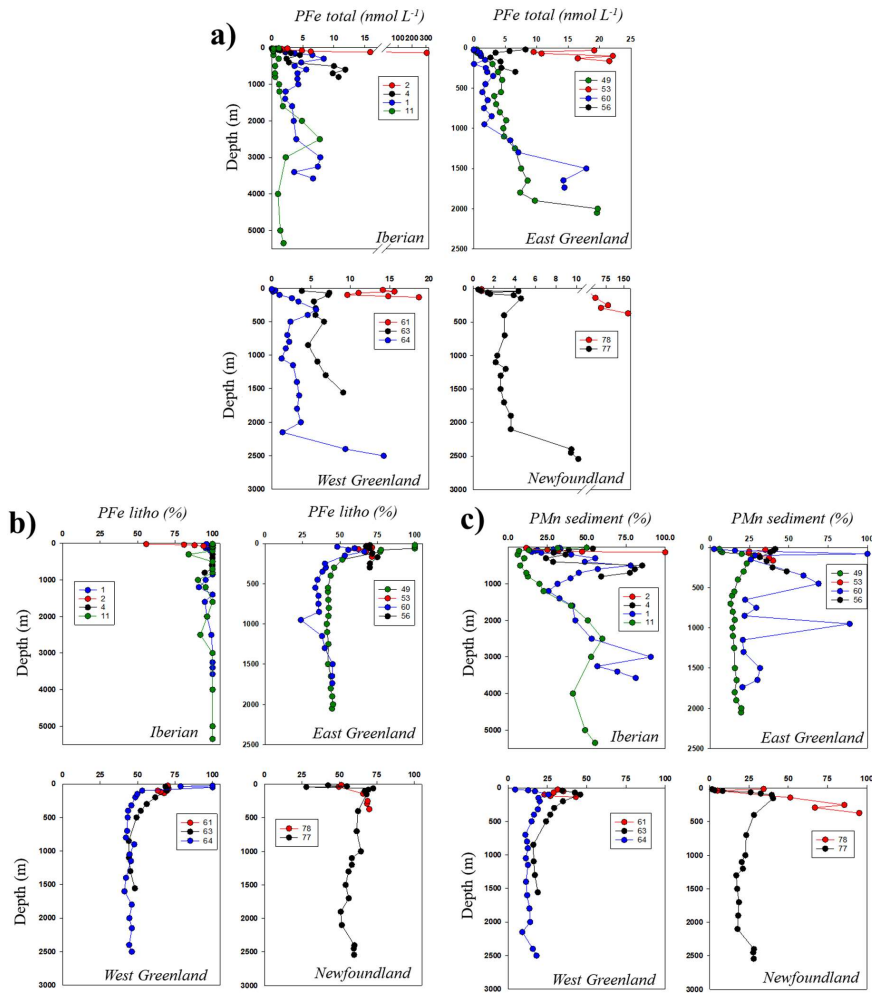
1223 Figure 9: Section of derived contribution of sedimentary inputs manganese bulk sediment proxy (a) and
 1224 transmissometry (b) along the GA01 section. Station IDs and biogeochemical region are indicated above the section
 1225 (a). This figure was generated by Ocean Data View (Schlitzer, R., Ocean Data View, odv.awi.de, 2017).



1226
 1227
 1228
 1229
 1230
 1231

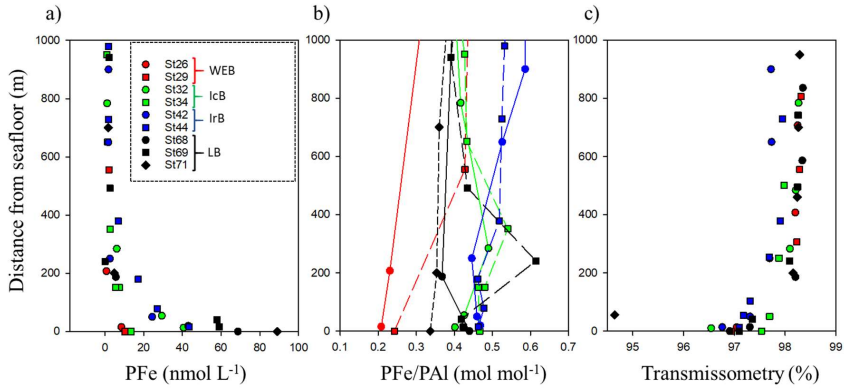
1232
1233

Figure 10: Vertical profiles of PFe (nmol L⁻¹, a), lithogenic proportion of particulate iron (%), b) and sedimentary proportion of particulate manganese (%), c) at the Iberian, East-West Greenland and Newfoundland margins.



1234
1235
1236
1237
1238
1239
1240

1241 **Figure 140:** PFe total (a); PFe/PAI ratio (b) and beam transmissometry (%) as a function of depth above the seafloor
 1242 (m) at selected stations where a decrease in transmissometry was recorded.



1243

1244

1245

1246

1247

1248

1249

1250

1251

1252

1253

1254

1255

1256

1257

1258

		Fe	Al	P	Mn
Blank (nmol L ⁻¹)	5µm filter	0.072	0.100	0.511	0.003
	0.45µm filter	0.132	0.164	1.454	0.005
Limit of detection (nmol L ⁻¹)	5µm filter	0.011	0.030	0.365	0.001
	0.45µm filter	0.026	0.046	1.190	0.001
Recovery CRM (%)	BCR-414 (n=10)	88 ± 7			94 ± 7
	MESS-4 (n=5)	98 ± 14	97 ± 14	80 ± 30	110 ± 18
	PACS-3 (n=8)	101 ± 9	99 ± 14	91 ± 34	112 ± 11

1259

1260 **Table 1: Blank and limit of detection (nmol L⁻¹) of the two filters and Certified reference material (CRM)**
1261 **recoveries during GEOVIDE suspended particle digestion.**

1262

1263

Author	Year	Fraction	Location	Depth range	PFe	PAI	PMn	PP
This study		>0.45µm	N. Atlantic (>40°N)	All	bdl-304	bdl-1544	bdl-3.5	bdl-402
Barrett et al.	2012	0.4µm	N. Atlantic (25-60°N)	Upper 1000m	0.29-1.71	0.2-19.7		
Dammshausser et al.	2013	>0.2 µm	Eastern tropical N.A.	0-200		0.59-17.7		
Dammshausser et al.	2013	>0.2 µm	Meridional Atlantic	0-200		0.35-16.1		
Lam et al.	2012	1-51 µm	Eastern tropical N.A.	0-600	ND-12			
Lannuzel et al.	2011	>0.2 µm	East Antarctic	Surface		0.02-10.67	0.01-0.14	
Lannuzel et al.	2014	>0.2 µm	East Antarctic	Fast ice	43-10385	121-31372	1-307	
Lee et al.	2017	>0.8 µm	Eastern tropical S.Pacific	All	bdl-159	bdl-162	bdl-8.7	bdl-983
Marsay et al.	2017	>0.4 µm	Ross Sea	All	0.68-57.3	ND-185	ND-1.4	5.4-404
Milne et al.	2017	>0.45µm	Sub-tropical N.A.	All	ND-140	ND-800		
Ohnemus et al.	2015	0.8-51 µm	N. Atlantic	All	0-938	0-3600		
Planquette et al.	2009	>53 µm	Southern Ocean	30-340	0.15-13.2	0.11-25.5		
Schlosser et al.	2017	>1 µm	South Georgia Shelf	All	0.87-267	0.6-195	0.01-3.85	
Sherrell et al.	1998	1-53µm	Northeast Pacific	0-3557		0.0-54.2		
Weinstein et al.	2004	>53 µm	Labrador Sea	0-250	0.1-1.2	0.1-1.5		
Weinstein et al.	2004	0.4-10µm	Labrador Sea	0-250	2.5	3.6	0.05	
Weinstein et al.	2004	>0.4 µm	Gulf of Maine	0-300	34.8	109		

1264

1265 **Table 2: Concentration (in nmol L⁻¹) of trace elements (PFe, PAI, PMn and PP) in suspended particles collected in**
1266 **diverse regions of the world's ocean. Bdl: below detection limit, ND: non-determined.**

1267

1268

1269